AD-A032 591 ARMY ENGINEER WATERWAYS EXPERIMENT STATION VICKSBURG MISS F/G 8/13
EVALUATING PENETRATION TESTS IN CLAY FROM MEASURED SOIL PARTICL--ETC(U)
FEB 71 Y T CHOU

UNCLASSIFIED WES-MP-71-2 NL

1 OF 1
AD-A
032 591

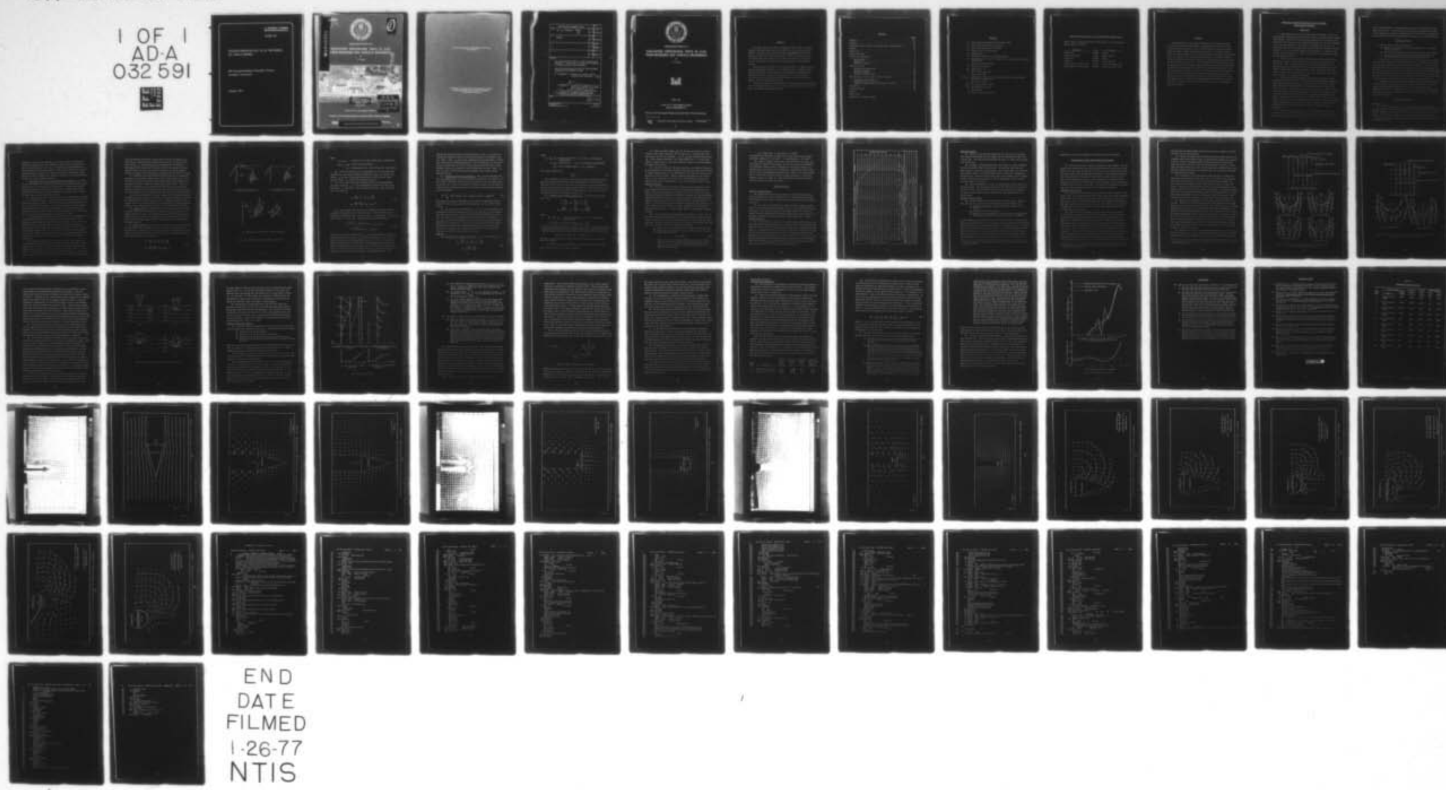

END
DATE
FILMED
1-26-77
NTIS

U.S. DEPARTMENT OF COMMERCE
National Technical Information Service

AD-A032 591

EVALUATING PENETRATION TESTS IN CLAY FROM MEASURED SOIL PARTICLE MOVEMENTS

ARMY ENGINEER WATERWAYS EXPERIMENT STATION,
VICKSBURG, MISSISSIPPI

FEBRUARY 1971

MISCELLANEOUS PAPER M-71-2

EVALUATING PENETRATION TESTS IN CLAY FROM MEASURED SOIL PARTICLE MOVEMENTS

by

Y. T. Chou

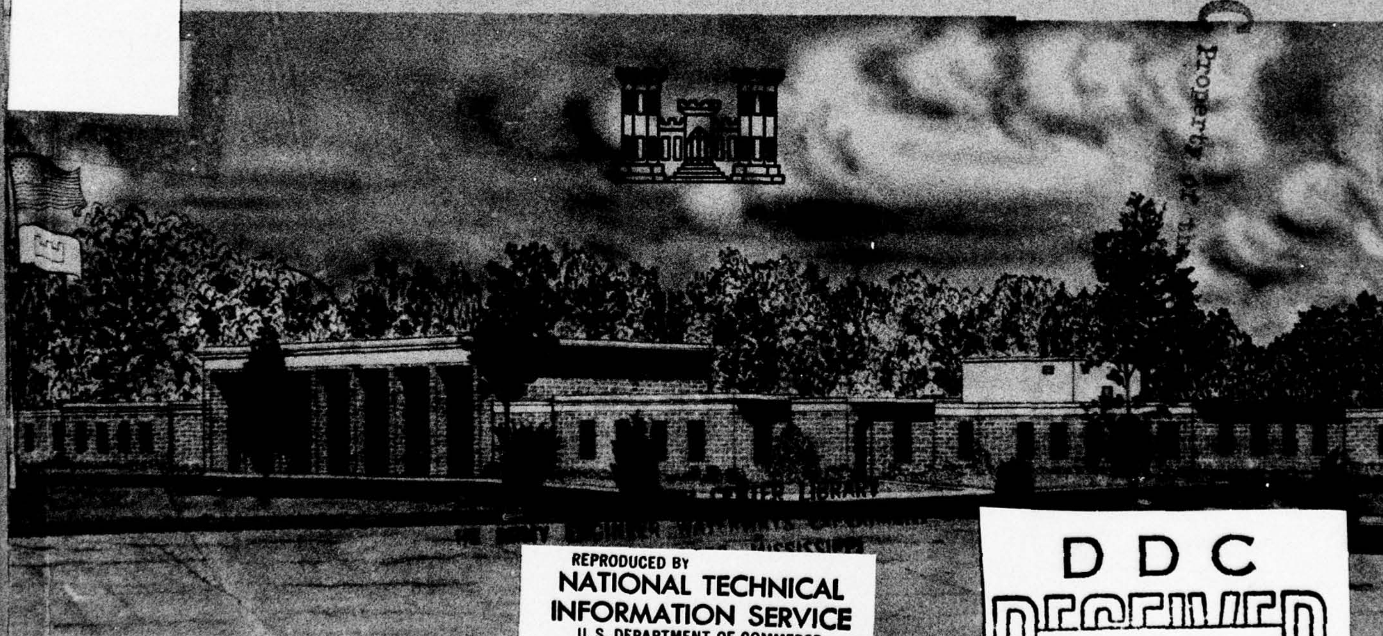

February 1971

Sponsored by U. S. Army Materiel Command

Conducted by U. S. Army Engineer Waterways Experiment Station, Vicksburg, Mississippi

ROUTING AND TRANSMITTAL SLIP

1 TO MR. W.G. SHOCKLEY (MESL) WGS	INITIALS		ACTION: CIRCULATE
	DATE		COORDINATION
2 LIBRARY	INITIALS		FILE
	DATE		INFORMATION
3	INITIALS		NOTE AND RETURN
	DATE		PER CONVERSATION
4	INITIALS		SEE ME
	DATE		SIGNATURE

REMARKS

DDC HAS REQUESTED MP-M-71-2 (COPY OF TITLE PAGE ATTACHED). WE ARE GOING TO SEND COPY ON LOAN AS NO RETENTION COPIES ARE AVAILABLE.

COULD YOU PLEASE TELL US WHICH OF THE FOLLOWING DISTRIBUTION STATEMENTS TO USE?

✓ STATEMENT A Approved for public release; distribution unlimited. WGS

OR

~~STATEMENT B: Distribution limited to U.S. Government agencies only; test and evaluation date ?. Other requests for this document must be referred to U.S. Army Materiel Command.~~

Do NOT use this form as a RECORD of approvals, concurrences, disapprovals, clearances, and similar actions

FROM LIBRARY BRANCH, TIC	DATE OCT 29 1976
	PHONE

OPTIONAL FORM 41
AUGUST 1967
GSA FPMR (41CFR) 100-11.206

5041-101-01

★ GPO : 1975-588-906

MISCELLANEOUS PAPER M-71-2

EVALUATING PENETRATION TESTS IN CLAY FROM MEASURED SOIL PARTICLE MOVEMENTS

by

Y. T. Chou

February 1971

Sponsored by U. S. Army Materiel Command
Project 1T061102B52A-01

Conducted by U. S. Army Engineer Waterways Experiment Station, Vicksburg, Mississippi

ARMY-MRC VICKSBURG, MISS.

This docu ... ~~or foreign nationals~~
may be m

Approved for Public Release; Distribution Unlimited

i

Foreword

The study reported herein was conducted in 1969 at the U. S. Army Engineer Waterways Experiment Station (WES) as a part of the vehicle mobility research program under DA Project 1T061102B52A, "Research in Military Aspects of Terrestrial Sciences," Task 01, "Military Aspects of Off-Road Mobility," under the sponsorship and guidance of the Research, Development and Engineering Directorate, U. S. Army Materiel Command.

The study was conceived and carried out by Dr. Y. T. Chou under the general supervision of Messrs. W. G. Shockley and S. J. Knight, Chief and Assistant Chief, respectively, of the Mobility and Environmental Division, and under the direct supervision of Dr. K. W. Wiendieck, former member of the Research Projects Group of the Mobility Research Branch. Dr. Chou prepared this report.

COL Levi A. Brown, CE, and COL Ernest D. Peixotto, CE, were Directors of the WES during the course of this study and preparation of this report. Mr. F. R. Brown was Technical Director.

Contents

Notation

c_t	Soil cohesion determined from triaxial tests
CI	Cone index (penetration resistance)
J_2	Second invariant of stress tensor
K	Yield stress in simple shear
P	Vertical load
R	Resistance of soil to a probe (constant)
u,w	Displacements of soil in r (radial) and z (vertical) directions, respectively
v	Velocity of soil movement
V	Penetration velocity
α,θ	Angles (fig. 1)
γ	Shear-strain component
Δ	Interval of time
$\varepsilon_r,\varepsilon_\theta,\varepsilon_z$	Strains in r (radial), (circumferential), and z (vertical) directions, respectively
σ	Normal soil stress
σ'_{ij}	Deviatoric stress tensor
σ_θ	Circumferential stress
τ	Shear stress
ϕ	Angle of internal friction

Conversion Factors, Metric to British Units of Measurement

Metric units of measurement used in this report can be converted to British units as follows:

Multiply	By	To Obtain
centimeters	0.3937	inches
square centimeters	0.155	square inches
millimeters	0.0394	inches
newtons	0.2248	pounds (force)
kilonewtons per square meter	0.145	pounds per square inch
kilonewtons per cubic meter	6.3659	pounds per cubic inch

Summary

The deformation and flow characteristics of a near-saturated fat clay under penetration were studied. Penetrations were made in a 50.8-cm-diam mold with a circular cone, a circular plate, and two rectangular plates at speeds ranging from 0.004 to 5.6 cm/sec. The strain, strain rate, and velocity fields in the soil were calculated from the soil particle movements, determined by measuring the displacement of pellets embedded in the soil before penetration. Actual soil flow patterns determined from velocity fields were studied. It was found that if the deformation energy of the soil were assumed equal to the penetration energy, the former could be obtained by integration over the affected volume of the deformed soil. The penetration resistance was thus computed on the basis of the Von Mises yield criterion and compared with the measured penetration resistance. Computed and measured penetration resistance values were markedly different; this casts some doubt on the applicability of the Von Mises equation to results of tests on clay under penetration and on the computational procedure employed.

EVALUATING PENETRATION TESTS IN CLAY FROM MEASURED SOIL PARTICLE MOVEMENTS

Background

1. Cone penetrometer tests have been used extensively at the U. S. Army Engineer Waterways Experiment Station (WES) to evaluate soil strength, and empirical correlations have been established between laboratory cone penetration resistance and tire performance parameters. The main advantage of the cone penetrometer is its inherent simplicity; but it must be recognized that basic soil properties, such as cohesion, internal friction, viscosity, etc., are not determined by this instrument. Therefore, the present trend in penetration studies heavily favors experimentation that yields empirical results.

2. Evaluation of cone penetration resistance of soil by relations based on the theory of continuum mechanics has not been particularly successful. Most of these analyses have been oriented toward static bearing capacity of footings and have not taken into consideration such factors as viscosity and inertia effects. Thus, while these theories assist somewhat in understanding the nature of a penetration test, they do not provide a means for evaluating it.

3. Recently, Yong[10] and Miller[6] developed a new approach toward rigid wheel-soil interaction. Using the concept of continuum mechanics, they approached the problem by an analytical-empirical method, visco-plasticity, which had previously been used successfully in analyzing metal processing. This method assumes that soil stresses under a wheel can be calculated if the velocity field within the soil is known. Yong and Miller determined the velocity field by sophisticated X-ray techniques. Strains and strain rates were computed, and the stress distribution was determined by a constitutive equation (the Von Mises plasticity equation) linking stresses and strain rates. Although this so-called visioplasticity method has yielded no conclusive results, it seems promising.

4. In the study reported herein, the visioplasticity method is applied to cone penetration tests. This problem is relatively simple compared to that of soil-wheel interaction. However, in contrast to the

work of Yong and Miller, the three-dimensionality of the problem is taken fully into account. It was hoped that the results would shed some light on the fundamental mechanics of penetration tests and allow the evaluation of the potential of the visioplasticity method for more complex problems.

Purpose and Scope

5. The purposes of this study were to:

   a. Study the deformation and flow characteristics of the soil under penetration.

   b. Examine the Von Mises equation in light of the test results.

   c. Evaluate the potential of the visioplasticity method for predicting soil-vehicle interaction theoretically.

6. Ten tests with four different probes--a circular cone, a circular plate, and two rectangular plates--were conducted in a 50.8-cm-diam* mold of heavy clay at speeds varying from 0.004 to 5.6 cm/sec. Only one soil was used; its moisture content averaged 50 percent, saturation ranged from 97 to 99 percent, and penetration resistance ranged from 38.8 to 129.5 kN/m^2. The strain, strain rate, and velocity fields in the soil were computed from the movements of soil particles. The movements were determined by measuring the displacement of pellets embedded in the soil before penetration.

7. Because of a lack of funds, the study was shortened and simplified considerably with respect to the original plan. Results from a circular cone and circular plate penetrating the soil at a very slow speed (0.004 cm/sec) were the only data used to compare measured and predicted penetration resistance, and results of the other tests are presented without further analysis.

Theoretical Background

Basic concept

8. In the basic concept of soil penetration problems in clay presented in this section, the validity of the theory of perfectly plastic solids and the selection of a relatively high-moisture-content clay for the test program are discussed. Also, the meaning of the velocity field and the

*A table of factors for converting metric to British units of measurement is given on page ix.

differences in the stress conditions in cases of plane strain and axi-symmetry are pointed out, with particular emphasis on the significance of the circumferential stress σ_θ. An equation is formulated based on the principle of energy conservation. This equation equates the rate of input penetration energy to the rate of output soil deformation energy, and can be used to evaluate the physical constants of the material numerically or to check available theories.

9. Validity of the theory of perfectly plastic solids. According to the Mohr-Coulomb law, shear stress increases with normal stress on the failure plane for all but purely cohesive soils. Drucker and Prager[3] generalized the Mohr-Coulomb law to account for all principal stresses, and Drucker[2] demonstrated that by applying the normality rule, a volume increase must accompany any plastic strain.

10. Upon application of a shear stress, soils undergo volume changes in a very complicated manner. Dense soils and overconsolidated clays increase in volume upon shear stress, but normally consolidated clays and loose sands decrease in volume. Also, sands can undergo further plastic strain without volume change once they have been strained far enough. Whitman[9] pointed out that the observed rates of expansion of dense sands are far less than those predicted from plasticity theory.

11. In discussing the importance and necessity of the normality rule, Whitman[9] quoted from a paper by Drucker, Gibson, and Henkel:[4] "The normality rule is much more than simply an assumption. It is the inevitable consequence of making two less stringent and very reasonable assumptions: (a) isotropy and (b) a stable material. Also, the important upper and lower bound theories are valid only so long as the normality ruls applies. Without the normality rule, we lose all theoretical justification for using such results as the Prandtl-Hill bearing capacity equations."

12. The general tendency in research on plastic flow problems of frictional materials is to retain the normality rule, but seek for other yield criteria. Strain rates do not remain normal to the Mohr-Coulomb yield surface, but are normal to another curved surface. The normality rule is satisfied if the curved surface is the yield surface. Drucker, Gibson, and Henkel[4] proposed that the yield surface for soils should look

like the Mohr-Coulomb surface, except that it should be capped at the open end by a dome that would expand and contract as the volume of the soil changed. In research conducted at Massachusetts Institute of Technology (MIT) for the WES,[1] the yield surface was assumed to be elliptical and to be able to move along the stress axis during plastic strain, the plastic volume changing in proportion to the change in stress.

13. Although the concept developed at MIT seemed to be reasonable and promising, conclusive results have not yet been established. It is felt that a correct plasticity theory solving plastic flow problems for frictional materials cannot be obtained in the near future. Since the theory of perfectly plastic materials has been found to be sound when applied to nonfrictional materials, this study was limited to soft clay at a consistency near full saturation, which satisfied the condition $\phi = 0$.

14. The clay tested had a moisture content of 50 percent, which was only about 3 percent short of saturation. The angle of internal friction ϕ determined from triaxial tests was zero. Although the high moisture content of the soil created difficulty and inconvenience in preparing the sample, it was overwhelmingly advantageous in the theoretical analysis.

15. Velocity field. Velocity fields in a soil mass show the directions and velocities of soil particle movements, or rather the flow or rupture patterns of soil. In this study, the velocity fields were computed from the measured soil particle movements, and the soil flow patterns under different shapes of probes penetrating at different speeds were investigated.

16. Stress conditions. Stresses on an element of soil in cylindrical and rectangular coordinates are shown in figs. 1a and 1b. In an axisymmetric case (fig. 1c), the stress components are independent of the angle θ, and all derivatives with respect to θ vanish. The strains and displacements have the relations

$$\varepsilon_r = \frac{\partial u}{\partial r} , \quad \varepsilon_\theta = \frac{u}{r} , \quad \varepsilon_z = \frac{\partial w}{\partial z}$$

$$\gamma_{rz} = \frac{\partial u}{\partial z} + \frac{\partial w}{\partial y} , \quad \gamma_{y\theta} = \gamma_{\theta z} = 0 \tag{1}$$

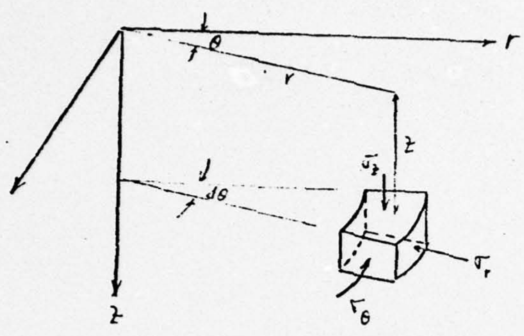

a. Cylindrical coordinates

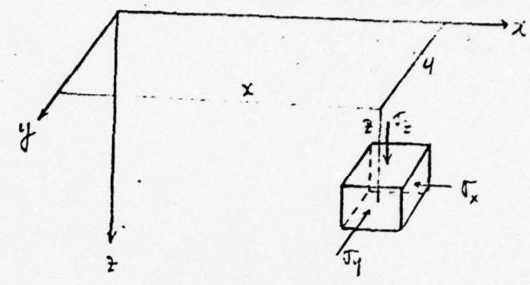

b. Rectangular coordinates

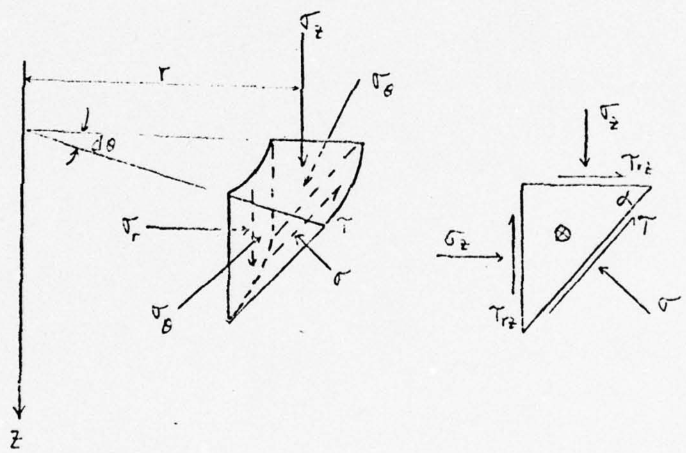

c. Stresses on an element in axisymmetric case

Fig. 1. Coordinate systems of stress components

where

$\varepsilon_r, \varepsilon_\theta, \varepsilon_z$ = strains in r, θ, and z directions, respectively

$\gamma_{r\theta}, \gamma_{rz}, \gamma_{\theta z}$ = shear-strain components

u, w = displacements in r and z directions, respectively

17. In the axisymmetric case, displacement in the circumferential direction is zero, since movement is confined to the r-z plane. But strain ε_θ in the circumferential direction is not zero and, consequently, stress σ_θ in the same direction exists.

18. In a plane strain case, displacement in the circumferential direction and strain ε_y in the longitudinal direction are both zero, but stress σ_y may exist. For the plane strain case, (fig. 1b), equation 1 has the form

$$\varepsilon_x = \frac{\partial u}{\partial x}, \ \varepsilon_y = 0, \ \varepsilon_z = \frac{\partial w}{\partial z}$$
$$\gamma_{yz} = \frac{\partial u}{\partial z} + \frac{\partial w}{\partial y}, \ \gamma_{y\theta} = \gamma_{\theta z} = 0 \tag{2}$$

19. In an axisymmetric case, it is possible to determine, by the condition of equilibrium, the normal stress σ and the shear stress τ on the line inclined to the r axis at angle α in terms of $\tau_{rz}, \sigma_r, \sigma_z$, and the angle α (fig. 1c). The equations can be formulated as

$$\sigma = \frac{\sigma_z + \sigma_r}{2} + \frac{\sigma_z - \sigma_r}{2} \cos 2\alpha - \tau_{rz} \sin 2\alpha$$
$$\tau = \frac{\sigma_z - \sigma_r}{2} \sin 2\alpha - \tau_{rz} \cos 2\alpha \tag{3}$$

Stresses on an oblique line in the r-z plane, therefore, do not depend on the circumferential stress σ_θ for the axisymmetric case. It was found that equation 3 is exactly the same for σ and τ in the plane strain state of stress.[5] Thus, the two-dimensional Mohr circle can be used to represent the state of stress for three-dimensional penetration problems in which the circumferential stress σ_θ can exist but does not influence the normal and shear stresses on the yield surface. The

maximum and minimum principal stresses must lie in the r-z plane for the axially symmetric state of stress since movement is confined to the r-z plane. Thus, σ_θ must be the intermediate principal stress. According to the Harr-Von Karman hypothesis,[11] the limiting state of stress at yield is reached when two of the three principal stresses--that is when two Mohr circles--are tangent to the limiting Mohr envelope. Thus, σ_θ must be equal to either the maximum principal stress or the minimum principal stress.

20. Principle of energy conservation. When a probe penetrates the soil at constant speed V, the rate of input energy is RV, where R is the constant resistance experienced by the probe. If it is assumed that the energy RV, which is a function of response behavior of the soil, is totally lost in deforming the soil, the following energy balance equation can be formulated.

$$RV = \int_{\overline{V}} (\sigma_r\dot{\varepsilon}_r + \sigma_\theta\dot{\varepsilon}_\theta + \sigma_z\dot{\varepsilon}_z + \tau_{r\theta}\dot{\gamma}_{r\theta} + \tau_{rz}\dot{\gamma}_{rz} + \tau_{\theta z}\dot{\gamma}_{\theta z})\, d\overline{V} \quad (4)$$

The expressions shown at the right are the rates at which the stresses deform the soil medium, and they are integrated over the affected soil volume.

21. In equation 4, the quantities R and V can be measured; and components of rate of strain tensor $\dot{\varepsilon}_r$, $\dot{\varepsilon}_\theta$, and $\dot{\gamma}_{\theta z}$ can be computed from the velocity field. With appropriate constitutive equations that link soil stresses to strain rates, the components of stress tensor σ_r, σ_θ, $\tau_{\theta z}$, etc., can be obtained in terms of strain rate, and the integration can be carried out. For tests at very slow penetration speeds, the Von Mises equations for perfectly plastic solids were used as the constitutive equation. The results of these tests are presented for future use, and the velocity fields are plotted.

Equations

22. Computation of strain rate fields. For an axisymmetric case,

$$\dot{\varepsilon}_r = \frac{\partial v_r}{\partial r}, \quad \dot{\varepsilon}_\theta = \frac{v_r}{r}, \quad \dot{\varepsilon}_z = \frac{\partial v_z}{\partial z}$$

$$\dot{\gamma}_{rz} = \frac{\partial v_r}{\partial z} + \frac{\partial v_z}{\partial \gamma} \quad (5)$$

where

$\dot{\varepsilon}_r$, $\dot{\varepsilon}_\theta$, $\dot{\varepsilon}_z$ = rates of strain in r , θ , and z directions, respectively

v_r , v_z = velocities in r and z directions, respectively

$\dot{\gamma}_{rz}$ = rate of shear-strain in r-z direction

For a plane strain case,

$$\dot{\varepsilon}_\theta = 0 \qquad (6)$$

23. Equations 5 and 6 are valid only for small deformations and are in a strict sense not accurate enough for problems with large strains. However, in view of present crude measuring techniques and other idealization of soil properties, it appears unrealisitc to include nonlinear terms in equations 5 and 6 to account for larger strains. Nevertheless, these equations were used for computing strain rates.

24. Levy-Von Mises plasticity equations. The Levy-Von Mises equations are:

$$\sigma'_r = \frac{K\dot{\varepsilon}_r}{\sqrt{I}} , \quad \sigma'_\theta = \frac{K\dot{\varepsilon}_\theta}{\sqrt{I}} , \quad \sigma'_z = \frac{K\dot{\varepsilon}_z}{\sqrt{I}}$$

$$\tau_{\theta z} = \frac{K\dot{\gamma}_{\theta z}}{2\sqrt{I}} , \quad \tau_{zr} = \frac{K\dot{\gamma}_{zr}}{2\sqrt{I}} , \quad \tau_{r\theta} = \frac{K\dot{\gamma}_{r\theta}}{2\sqrt{I}} \qquad (7)$$

where

σ'_r , σ'_θ , σ'_z = stress deviations* in r , θ , z directions, respectively

$I = 1/2\ (\dot{\varepsilon}_r + \dot{\varepsilon}_\theta + \dot{\varepsilon}_z) + 1/4\ (\dot{\gamma}_{\theta z} + \dot{\gamma}_{zr} + \dot{\gamma}_{r\theta})$

---

* It is frequently convenient to decompose the stress tensor into a spherical part corresponding to the mean normal stress and a deviatoric part. The stress deviation is defined as the tensor with the normal components

$$\sigma'_r = \sigma_r - s , \quad \sigma'_\theta = \sigma_\theta - s , \quad \sigma'_z = \sigma_z - s$$

and the same shearing components as the stress tensor. The mean normal stress is defined:

$$s = 1/3\ (\sigma_r + \sigma_\theta + \sigma_z) = 1/3\ (\sigma_x + \sigma_y + \sigma_z) = 1/3\ (\sigma_1 + \sigma_2 + \sigma_3),$$

which is ~~an~~ the first invariant of the stress tensor.

25. These equations assume that (a) the rate of strain is proportional to the stress deviation, (b) the material is incompressible and nonviscous, and (c) the condition $J_2 = K^2$ is never violated during flow. (J_2 is the second invariant of the stress deviator tensor and K is the yield stress in simple shear.) This last condition implies that work-hardening phenomena do not exist.

26. Since the test soil was near saturation and could be assumed to be incompressible, hydrostatic stresses would not cause any soil straining or energy dissipation, i.e. the hydrostatic stress did not influence the deviatoric stress behavior. Hence, in energy computations, as in equation 4, it was necessary to consider only the deviatoric component of stress, which can be represented by σ'_{ij}, the deviatoric stress tensor.

Material constants

27. In the theoretical analysis of soil mechanics problems, it is very difficult to evaluate the material constants from laboratory test data. These constants depend on a number of factors, probably the most important being the difference in the stress systems, i.e. the laboratory-determined material constants are based on ideal loading conditions that usually do not represent the real conditions under a complex state of stress. If it is assumed that the laboratory triaxial test results can be used to determine soil strength, $K = (\sigma_1 - \sigma_3)/\sqrt{3}$ when the Von Mises yield condition is used. $K = (\sigma_1 - \sigma_2)/2$ when the Tresca yield condition is used.

28. In this study, the Von Mises yield criterion was used. The K value was not determined directly from the triaxial tests, which are difficult and expensive to run at such high moisture contents, but by extrapolations from previous triaxial and cone penetration test results with the same soil. This was done by the following procedure:

a. Determine the cone penetration resistance of the test soil.

b. Obtain the value of the cohesion of the test soil from the empirical relation,[8]

$$CI = 12.5\ c_t \tag{8}$$

where CI is the cone index of the soil and c_t is the cohesion of the soil determined from triaxial tests, which is equal to $(\sigma_1 - \sigma_3)/2$. (Equation 8 was plotted in pounds per square inch in fig. 5 of reference 11, but may be used for other units.)

c. Compute the K value from $K = 2c_t/\sqrt{3}$.
The penetration resistance of the test soil was found to be 55 kN/m^2 , yielding a cohesion of 4.4 kN/m^3 . K was computed as 5.1 kN/m^2 .

29. Based on results of numerous tests on both fat and lean clays with moisture contents of 45 percent or less (no tests were conducted at 50 percent moisture content comparable to the present study), the relation shown in equation 8 was formulated. Although the error caused by the linear extrapolations beyond the test range is not exactly known, the K value thus obtained should be fairly reasonable. It is very doubtful, however, if this K value is exactly the yield stress that occurred in the soil under penetration.

Laboratory Tests

Soil and its preparation

30. The fat clay used in this study was river alluvium obtained near Vicksburg, Miss., and was classified CH according to the Unified Soil Classification System. Gradation and classification data are shown in fig. 2.

31. The soil was air dried to a uniform moisture content, crushed with a hammer mill, and sieved through a 0.3-cm screen before being mixed with water. The soil and water were thoroughly blended in a pug mill until a uniform consistency was obtained, after which it was stored in an airtight container for about 24 hr before being molded into a sample.

Sample preparation

32. A test sample was prepared in a 50.8-cm-diam mold that could be separated vertically into two halves. Processed soil was compacted in the mold with a mechanically operated, 127-N, wedge-shaped drop hammer falling 15.2 cm. A 1-cm-thick rubber mat was placed over the surface of the soil, but it was lifted occasionally to prevent its sticking to the soil and blocking the free release of air. A sample was made up of 20 layers, each receiving 400 blows of the compaction hammer uniformly over the surface. With this procedure, it is believed that the sample achieved uniformity, and a maximum amount of air was expelled from the soil.

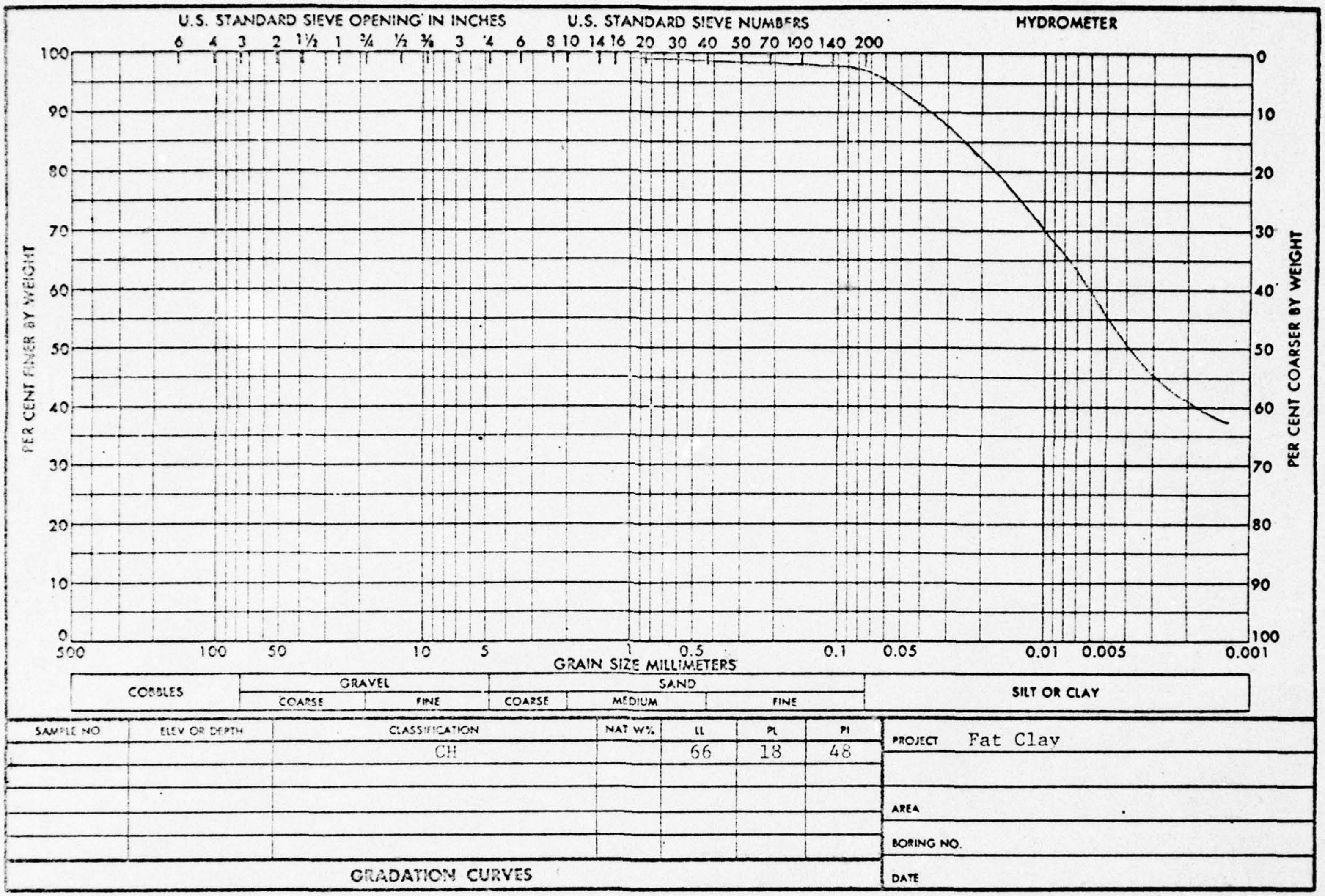

Fig. 2. Soil classification data

Testing procedure

33. After the soil had been compacted, the two halves of the mold were slightly disengaged, and the sample was cut vertically in half with a piano wire. The mold was disassembled and laid on a table with the flat soil surface up.

34. Straight, orthogonal grid lines were drawn at 1.27-cm intervals on the soil surface with a sharp pencil. At locations where the grid lines would be destroyed by penetration, small colored pins were inserted. The complete pattern of the grid lines then was traced on a transparent plastic sheet. After the soil surfaces were oiled lightly, the two halves of the mold were put back together, and the penetration tests were made near the center of the mold.

35. After penetration, the mold was disassembled and the halves were separated again. The deformation pattern of the grid lines was traced on the same plastic sheet.* Where the lines were destroyed by penetration, the areas could be reconstructed readily by the new positions of the colored pins.

Accuracy of test method

36. The test method used in this study was rather crude. Factors that affected the reproducibility of test results were found to be:

a. Variation (within ±2 percent) in moisture content of the samples.

b. Nonuniformity of the samples.

c. Variation in the penetration technique (i.e. a slight eccentricity of the penetration could not always be avoided).

In two different soil samples prepared and penetrated under identical conditions, the penetration resistance values were very close, but the deformed grid lines (or the soil flow patterns) were not exactly the same. In other words, the displacement of a soil particle at a particular location in one soil sample was not the same as in the same location in a second sample. However, this did not seem to constitute a problem in this study, because the computations were based on integration over the total volume of the

* In both axisymmetric and plane strain cases, soil particles moved only in the cut plane.

deformed soil and did not depend on individual particle movements.

Presentation of Test Results and Their Analysis

37. The results of this study are presented in three parts: (a) laboratory test results that show the flow characteristics and particle movement of the soil under penetrations, (b) the computer program, and (c) the theoretical prediction of penetration resistance. The penetration resistance was predicted by assuming the deformation energy of the soil to be equal to the penetration energy, and an integration of the deformation energy over the total affected volume of the deformed soil was carried out to obtain the penetration resistance. The computed penetration resistance then was compared to the measured cone penetration resistance.

Laboratory test results

38. Representative laboratory test results are shown in table 1 and plates 1-10. Nonhomogeneity of the test soils could not always be avoided, so the deformation patterns on opposite sides of the probe were usually dissimilar. This was reasonable because the load tended to deform most on the side that offered the least resistance. Occasionally, the magnitude of displacement at a distant point was found to be greater than that at a point closer to the probe.

39. Test results for a 30-deg circular cone with a base area of 2.3 cm^2 (5.4 cm in diameter) are presented in plates 1-4. Penetration speed was 5.6 cm/sec, the highest used. (The pins near the cone in plate 1 were placed after the test to provide a better contrast in the photograph; this was found later to be unnecessary.) The affected zone was rather small, and soil beneath the tip of the cone seems not even to have moved. The stream lines (flow paths) of soil particles are shown in plate 2. Plate 3 is the complete trace of soil particle movements at the grid points from the time when the cone was just touching the soil surface until the end of the test.* The displacement vectors of soil of soil particles at grid points around the cone are presented in plate 4;

* This result was obtained by assumption of steady state, which is discussed in paragraph 45.

the starting and ending points of each arrow show the original and final positions of the soil particles.

40. Results of tests with a 5.1-cm-diam circular plate moving at an extremely slow speed (0.004 cm/sec) are presented in plates 5-7, and with a 3.8- by 22.8-cm rectangular plate at the same speed in plates 8-10. (The pins shown in plates 5 and 8 were placed before the tests.) Under this slow penetration speed, the soil was generally assumed to behave as a perfectly plastic material, an assumption that did not necessarily apply to fast penetration speeds.

41. The portion of soil that moved with each plate is termed the soil nose in this report. Soil noses under the circular plate penetrating at four different speeds are shown in figs. 3b-3e, and under the 5.1- by 25.4-cm rectangular plate at two different speeds in figs. 4b and 4c. Figures 3a and 4a show the locations of pellets embedded in the soil and the original grid lines before penetration. The soil nose formed under the 5.1- by 25.4-cm rectangular plate by penetration at a very slow penetration speed (fig. 4b) had a triangular shape, but changed to circular as the speed was increased to the standard 3.1 cm/sec (fig. 4c).

42. Soils in the vicinity of the soil noses experienced large shear strains. Because of the adhesion force between the plates and the soil, the portion of soil near the plates did not move away, but moved vertically downward with the plate like a rigid body. This may be verified by the position (relative to the plate) of pellet No. 4, which was 1.27 cm below the center of the plate before and after penetration in all tests. Pellet No. 1 did not move away in any of the tests; pellet No. 2 moved slightly in some tests in which the soil conditions on the right side of the mold were apparently weaker than on the left. Pellet No. 8, which was placed at a depth half the width of the plate (2.54 cm) below the center of the plate, was lost in most tests.

43. Deformation patterns were distinctly different in cases of plane strain and axisymmetry. In the plane strain case (plates 8, 9, and 10*), the deformations were extended to a large area; the soils along the edge

* These tests with an elongated plate (3.8 by 22.8 cm) can be considered plane strain tests.

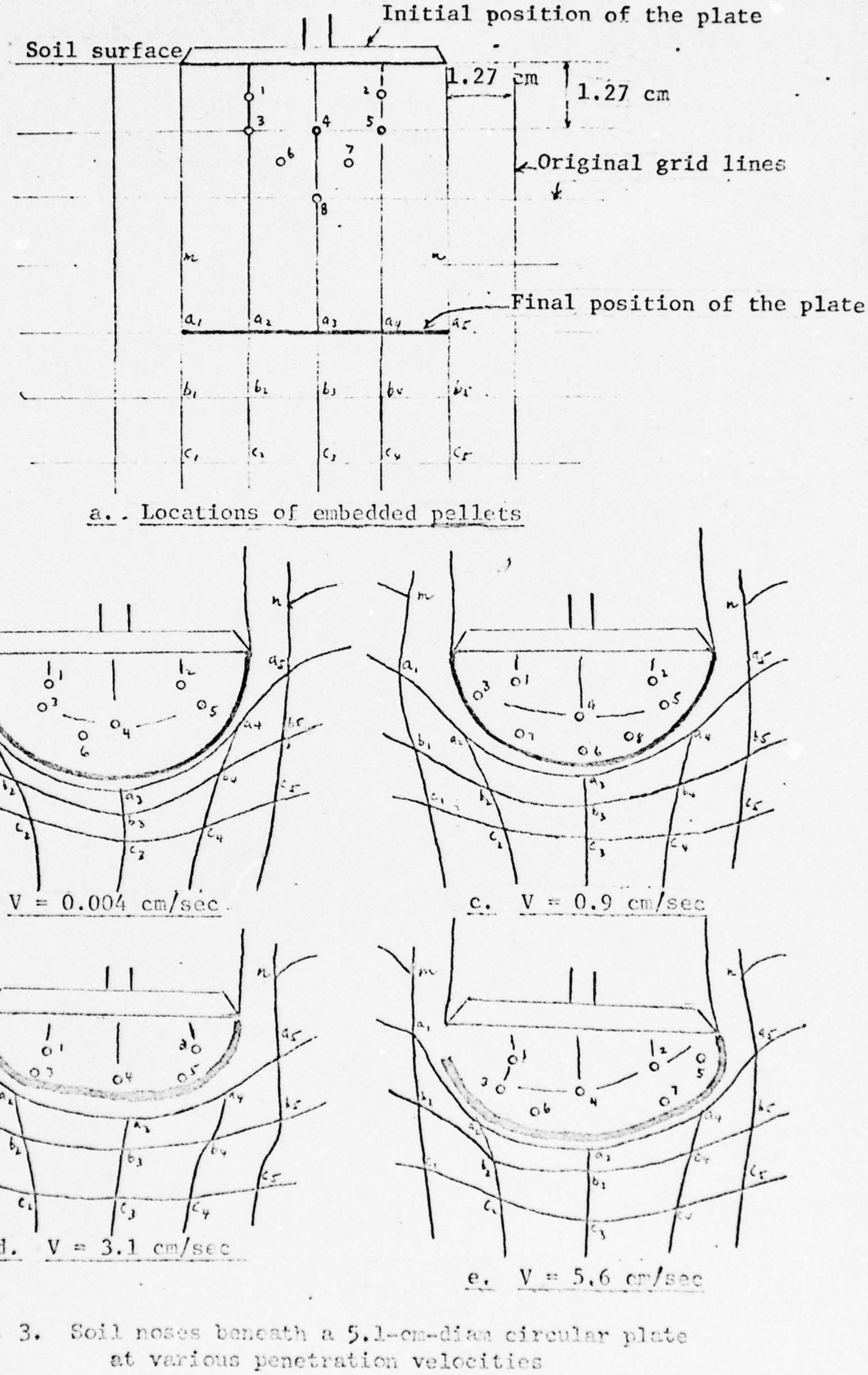

Fig. 3. Soil noses beneath a 5.1-cm-diam circular plate at various penetration velocities

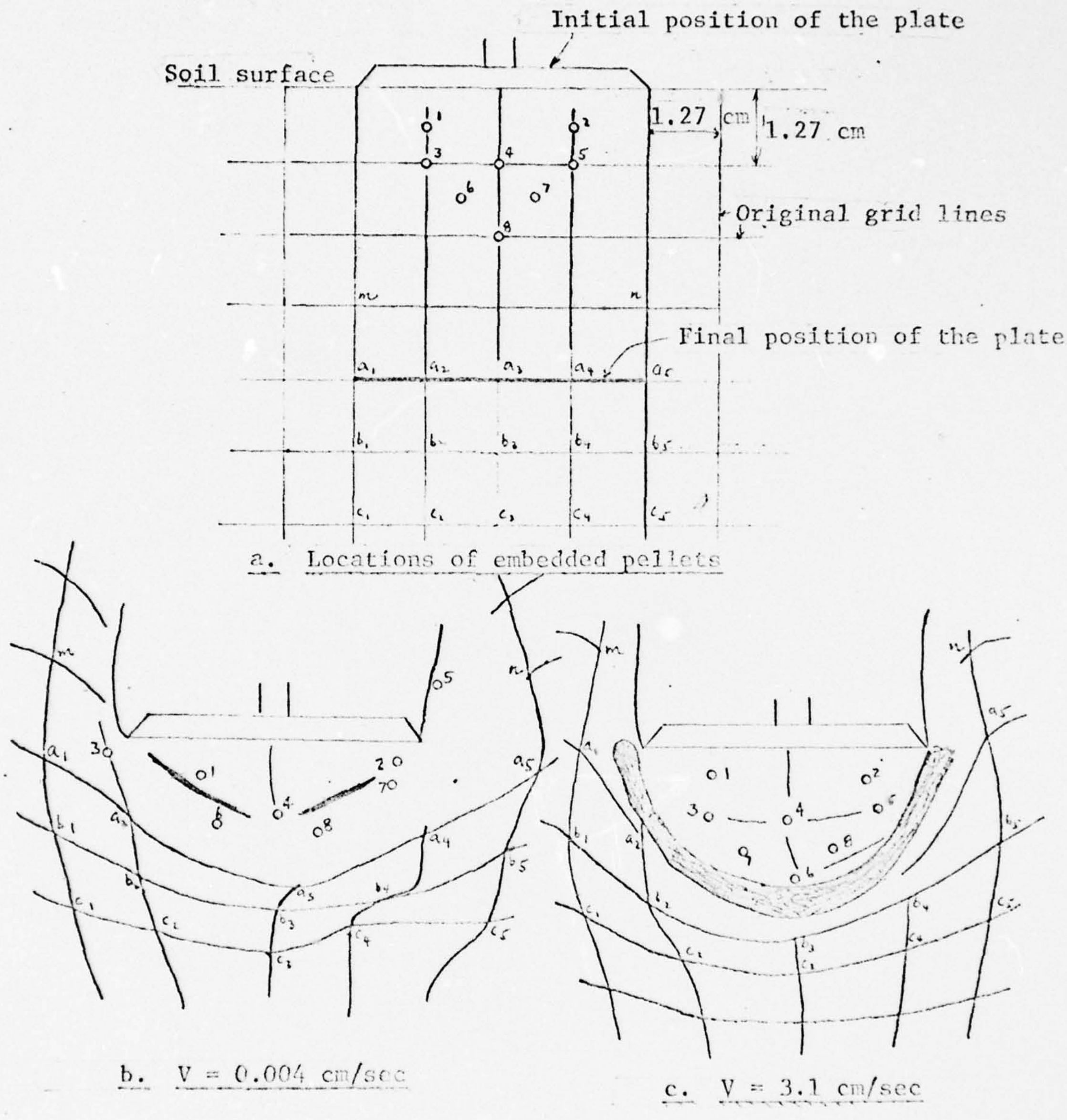

Fig. 4. Soil noses beneath a 5.1- by 25.4-cm rectangular plate at two different penetration velocities

of the mold were heaved slightly, indicating the mold actually was not large enough for the deformation patterns to be complete. The soil evidently was failed by shear stresses, the failure lines showing clearly in plate 8. Although the soil was failed by shear stresses in the axisymmetric case (plates 5 and 7), no rupture lines can be seen. This soil responded to penetration as viscous fluids might, and the soil deformations were limited to small areas near the plate. Despite these differences, the unit penetration resistances for these cases were not very different from each other, as shown in table 1. When the flow patterns in plates 1 and 5 are compared, it can be seen that penetration speed had no effect on soil deformation patterns in the axisymmetric case. In the plane strain case, however, the failure lines are still seen at a penetration speed of 3.1 cm/sec, but not as clearly as at slower penetration speeds.

44. The soil flow patterns in the zone near the penetration hole were not exact because the soil here tended to flow toward the hole by gravity. This lateral soil movement occurring during and after the penetration gave false information for computed results of strain rate fields. The magnitude of this error, however, could hardly be evaluated.

45. To trace the continuous movements of soil particles under penetration, the deformed grid lines are recorded as a function of time. This can be done by: (a) the X-ray method used by Yong[10] and Miller,[6] and (b) the measurement of deformed grid patterns in identical soil samples penetrated at different depths. The first method could not be used for this study because X-ray facilities for testing large samples were not available at the WES. The second method was not used because a large number of tests are required, and identical soil samples are very difficult to prepare. Instead, steady state of movement of soil particles was assumed; this allowed the continuous soil particle movement to be deduced from the final positions of the deformed grid lines. Actually, the validity of the use of the superposition technique to trace the entire history of soil particle movements is thus assumed.

46. The grid lines in a test sample being penetrated by a cone are shown schematicaly in fig. 5. The horizontal lines before penetration are shown in fig. 5a, and the deformed patterns at successive times in figs. 5b, 5c, and 5d. Under assumed steady state, line 3-d should have

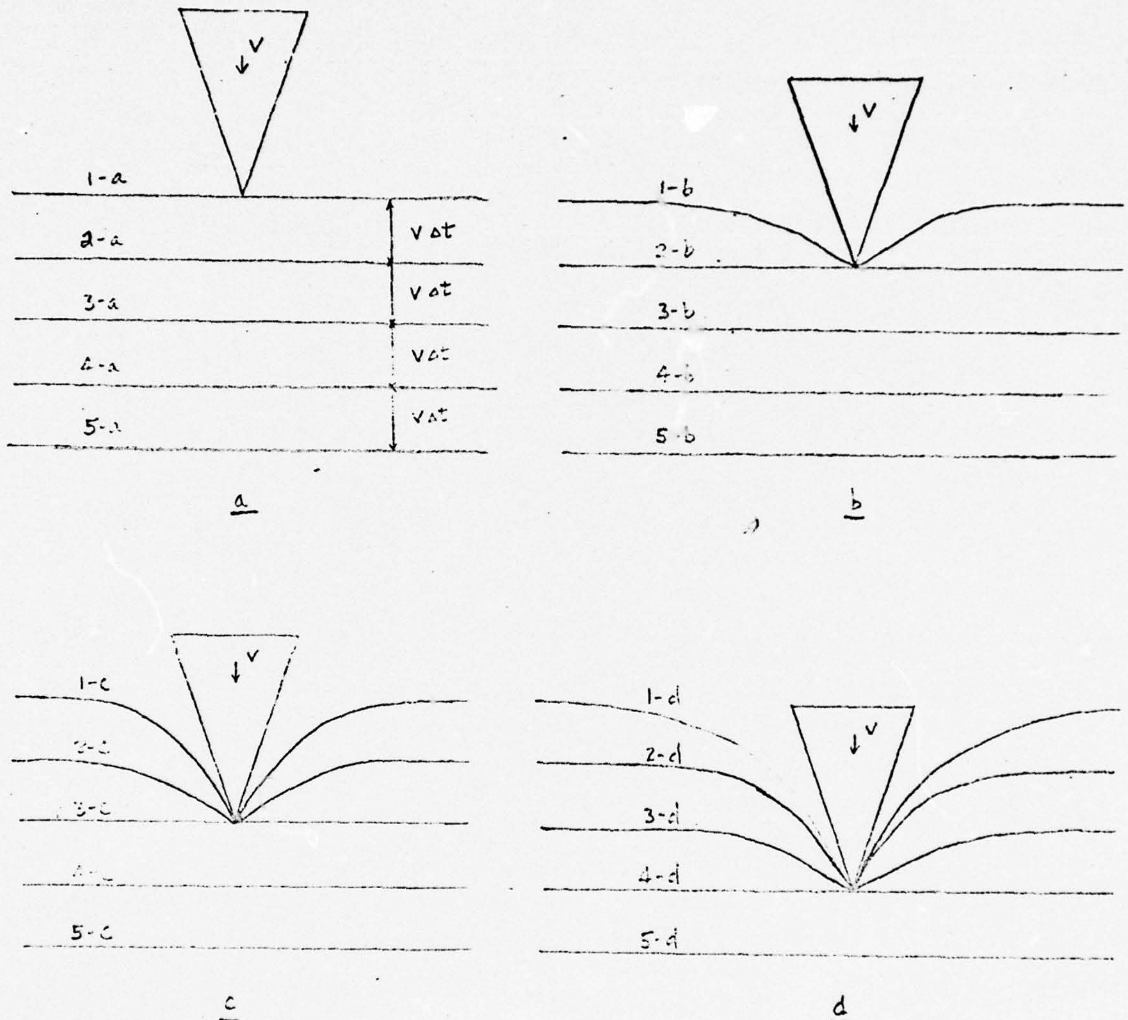

Fig. 5. Steady-state penetration of soil sample

the same shape as lines 2-c and 1-b; also, line 2-d should have the same shape as line 1-c. As the cone penetrates further into the soil, the deformed lines surrounding the cone should have the same shape as those at Δt time ago. In other words, the patterns of deformed lines are independent of depth, just as the waves surrounding a sailboat do not change as long as the boat is moving at constant speed.

47. Experimental results obtained at the WES[8] have shown that penetration resistance of clay does not depend upon penetration depth, except for small variation due to overburden. The strength of the soil surrounding the probe does not change as the probe penetrates the soil so the soil can be assumed to be a uniform and homogeneous medium with constant strength. Hence, the assumption of steady state for the cases investigated herein seems to be valid.

Computer program and results

48. A computer program (Appendix A) was prepared to be used for predicting penetration resistance of the soil. It was written in three parts:

a. Computation of velocity field.

b. Computation of strain rates at grid points.

c. Computation by the Von Mises equation of the stress components at each grid point and the rate of stresses deforming the soil

Based on the energy balance equation 4, the validity of the Von Mises equation was checked. The numberical value of soil yield stress was determined by laboratory triaxial tests previously conducted.

49. The essential work in the program was to compute the strain rates at the grid points. Equations 5 and 7 were used for this purpose with the input data measured from test results.

50. The original grid lines (solid) and the stream lines (dashed) are shown in fig. 6a; fig. 6b shows the complete trace of soil particle movement at each grid point, from time $t = 0$ to $t = 5\Delta t$ where Δt is the time required for the cone to move through the distance D. The displacements in r and z directions, as a function of time t, are presented in figs. 6c and 6d, respectively. There are various ways to compute the velocity field and strain rate field. That used to compute a velocity field is as follows:

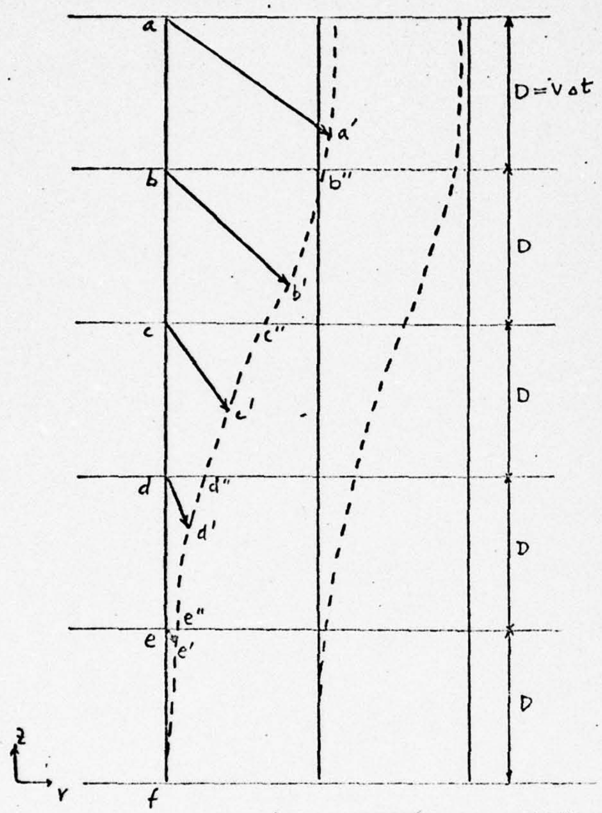

a. Original (solid) and stream (dashed) lines

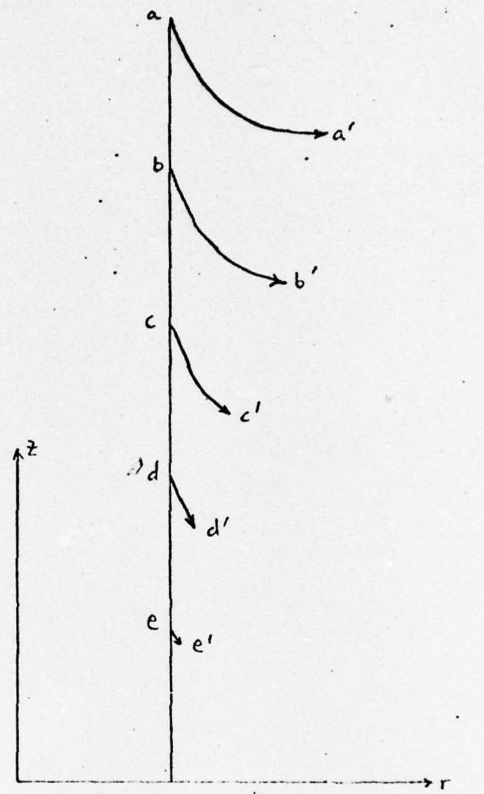

b. Soil particle movements at grid points

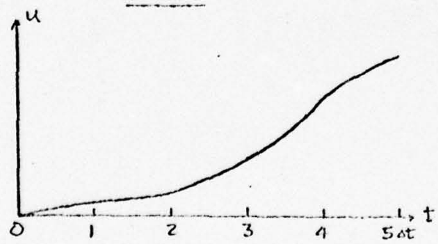

c. Displacement in radial direction

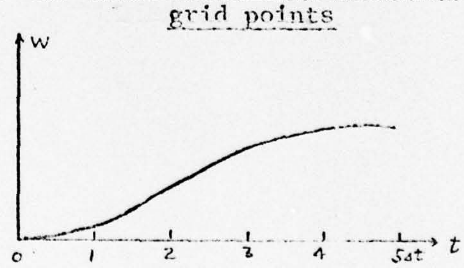

d. Displacement in vertical direction

Fig. 6. Data reduction

a. The locations of deformed grid points, i.e. a' , b' , c' , d' , e' , and f' (fig. 6a), were first read into the computer. The measurements were taken with reference to a fixed coordinate system.

b. The displacements u and w were computed according to the definition $(u \text{ or } w)_{t_o \to t}$ = total displacement up to time t minus displacement at time t_o .

c. An n-th order polynomial based on the least square technique was generated by the computer and represented the displacement versus time curves. The slopes of the curves at time $t = \Delta t$, $2\Delta t$, $3\Delta t$, $4\Delta t$, and $5\Delta t$ resulted in velocities corresponding to points e' , d' , c' , b' and a' , respectively (fig. 6a). It was found that polynomials with an order of 8 would fit most data with an acceptable degree of accuracy.

51. To compute a strain rate field, the following steps were taken:

a. Based on values of velocities at points a' , b' , c' , d' , and e' along a stream line, velocities at points b" , c" , d" , and e" were obtained. These points were actually the intercepts of the stream line on the undeformed horizontal grid lines.

b. After these velocities had been obtained for all stream lines, the velocities at each intersection on the undeformed grid were generated by the computer, and the horizontal and vertical components of the velocities, as well as the rate of change of velocities in both directions, were determined by the least square method in conjunction with polynomials. Thus, the strain rate tensor $\dot{\varepsilon}_{ij}$ at each grid point was obtained.

52. Difficulty was encountered, however, in using the least square procedure in paragraph 51b. According to computer print-outs, velocities did not always increase or decrease monotonically, but fluctuated in one direction. For example, velocities along a vertical grid line below the probe did not always decrease with depth. It was found that the variation in the order of polynomials was very sensitive to the variation in velocity values. The correct order for a given set of data could not be determined analytically by any method except trying a series of different values. In this program, orders from 3 to 14 (less than the data points) were tried, and the one that gave the best approximation was selected in the computation.

53. A velocity field shows the flow pattern of soil under

penetration. The velocity fields beneath probes at the moment penetrations were completed are depicted in plates 11-16. (Since steady-state conditions were assumed, the same velocity field should be observed at any other stage of penetration.) The arrows shown indicate the magnitude of velocity and direction of movement of soil particles, and the dashed lines show the stream lines. These lines indicate the directions of maximum shear stress.[7] Along the stream lines, velocities of soil particles were relatively large close to the probe, but became smaller as the distance increased from the probe. In other words, the velocity decreased along each stream line. The rates of change of velocity (or strain rate) along the stream lines at slow penetration speed (plates 11, 13, and 15) were observed to be smaller than those at faster penetration speeds (plates 12, 14, and 16). Since the deviatoric stress is proportional to the strain rate, according to the Von Mises concept, the stresses along equivalent stream lines should be greater under faster penetrations than under slower ones. This is reasonable because experimental results revealed that the penetration resistance increased with increasing penetration speed.

54. It is interesting to note that soils under penetration do not move along a unique slip surface in the velocity fields as most theoretical analyses have assumed (fig. 7). It usually is assumed that at the time of

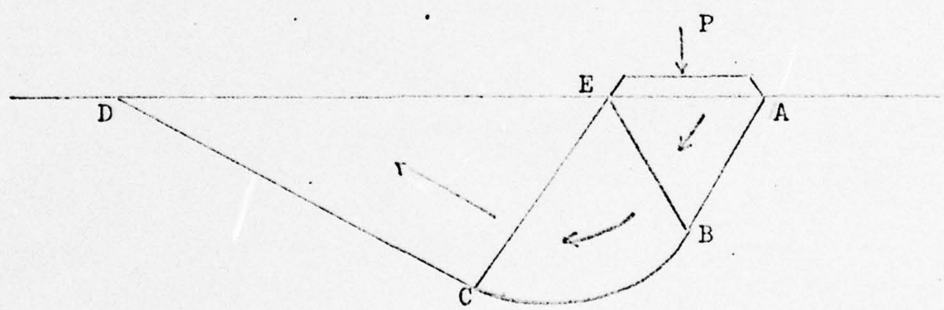

Fig. 7. Soil movements beneath a footing

failure, soils beneath the failure surface ABCD do not move at all, while soil masses in portions ABE and ECD slide to the left like a rigid body along surface ABCD without internal energy dissipation. Energy is dissipated along the surface ABCD and within the fan BCE . This was not

the case, however, for the cases in this study: The velocity varied along the stream line and also among stream lines; also, the grid squares were distorted after movement (plates 1, 5, and 8), indicating that there were relative displacements among soil particles that moved along infinite numbers of surfaces rather than along a unique surface.

55. It is important to realize that the assumption of rigid body movement of a soil mass beneath a footing applies to the condition of incipient failure or limit equilibrium, i.e. the initial movement of the soil mass at the beginning moment of failure. With continued movement, as in this study, the soil mass may deviate from the simple rigid body.

56. The computed velocity field beneath a 3.8- by 22.8-cm rectangular plate moving downward at a very slow speed (0.004 cm/sec) (plate 15) can be compared with the rupture lines in the soil sample after the test (plate 8). It appears that the computed directions of soil particle movement checked quite well with the observed direction or rupture lines, indicating that the computation method for velocity fields employed in this study was reasonably accurate.

57. In the velocity field beneath a 5.1- by 25.4-cm rectangular plate moving downward at a speed of 3.1 cm/sec (plate 16), the stream lines (velocity field) appear to be different from those in plate 15. At slow penetration speed (plate 15), the soils moved away from the probe in a markedly horizontal direction; whereas at faster speed (plate 16), soil near the probe moved in a markedly vertical direction.

58. Velocity fields beneath a 5.1-cm-diam circular plate at penetrating speeds of 0.004 and 5.6 cm/sec are shown in plates 13 and 14, respectively. The velocity fields differed under these two speeds, as did those in plates 15 and 16, and the same discussions apply. As the penetration speed increased, the stream lines generally became steeper, and the distance from the probe to the ends of the flow lines decreased.

59. Plates 11 and 12 are similar to plates 13 and 14, except that a 5.4-cm circular cone was used. Because of the sharp apex angle of the cone, soils beneath the cone tip were hardly moved. Otherwise, the discussions previously made for other types of probe are also applicable to results with this one.

Theoretical prediction of penetration resistance

60. The procedure for computing the penetration resistance based on the measured strain rate fields is given in this section. The computer results were limited to the axisymmetric cases at very slow penetration speeds (Nos. 1 and 2 in table 1).

61. With the velocity components at each grid point known, the components of strain rate can be computed; with the proper constitutive equation for the soil, the total resistance of the soil can be evaluated by equation 4 (the energy balance equation) and theoretically should be equal to the measured penetration resistance. In using equation 4 to carry out the integration, only the affected soil volume beneath the probe was considered; the effect of soil above the probe was discarded. This simplification was assumed as a direct consequence of the steady-state assumption; it reduced the effect of the soil above the probe to simple overburden pressure, which was insignificant in the investigated cases since the penetration resistance in clay remained almost constant after full penetration of the probe. Also, the soil above the probe tended to move toward the penetration hole, resulting in unrealistic and false velocity and strain rate fields insofar as the prediction of penetration resistance was concerned.

62. To save computer time, it was assumed that the deformation energy in the soil under penetration was symmetrical with respect to the probe. Consequently, the computations were carried out for one half of the mold only. In the analysis, the Levy-Von Mises plasticity equation was used. The soil yield stress K was taken as 5.1 kN/m^2 (paragraph 28). The soil resistances computed from the measured strain rate fields were very much larger than the measured penetration resistances, as shown in the following tabulation.

Test No.	Probe	Penetration Speed cm/sec	Measured Resistance N	Computed Resistance N	Computed Soil Yield Stress K kN/m^2
1	5.1-cm circular plate	0.004	110	680	0.76
2	5.4-cm circular cone	0.004	133	431	1.53

63. If the theory of plasticity is assumed to be valid for frictionless materials, and if the measuring technique and the computed strain rates are assumed to be reasonably accurate, questions may arise as to whether the numberical value of soil yield stress K used in computations is properly chosen. In the Levy-Von Mises equation, K is defined as the yield stress in shear, or $1/\sqrt{3}$ yield stress in tension or compression. It is, of course, questionable whether the yield stress determined from the laboratory triaxial test can represent the yield stress under the complex state of stress in the soil sample under penetration. If the computation including the simplifying assumptions is reasonable, the real soil yield stress K under penetration may be computed by equation 4. Substituting the Levy-Von Mises plasticity equation 6 into equation 4 yields

$$RV = K \int_{\bar{V}} (\dot{\varepsilon}_r^2 + \dot{\varepsilon}_\theta^2 + \dot{\varepsilon}_z^2 + \frac{1}{2}\dot{\gamma}_{rz} + \frac{1}{\sqrt{I}}) \, d\bar{V} \tag{9}$$

Since R and V are measured and the components of the strain rate tensor can be computed, the soil yield stress K under penetration can be computed from equation 9. These values are listed in the last column of the tabulation in paragraph 62.

64. The large discrepancies between the measured and computed penetration resistance values in these two tests may be explained by:

a. The soil was nonuniform, i.e. the deformation patterns at the cut surface did not well represent those on other surfaces.

b. The Levy-Von Mises equation was inadequate for describing the soil behavior under penetration, i.e according to the Von Mises equation, it is reasonable to believe that the rate of strain is proportional to the stress deviation during flow, but it is questionable whether the yield condition $J_2 = K^2$ is always valid during flow. Also, the soil samples were not exactly incompressible, which violates the basic assumption of Von Mises equation.

c. Errors were caused by the high-order polynomial approximations, i.e. in the computer calculations, the measured displacement data were fed into the computer without first being smoothed. A polynomial with higher order was desirable to approximate the relation of displacement to time. Although a high-order polynomial may be able to approximate the displacement-time relations with fair precision, the

derivatives of the polynomial would deviate very much from those of the displacement-time relation due to the oscillating nature of the high-order polynomial. This may best be explained by an example. The solid line connected by crosses in fig. 8a shows the measured displacement-time relation of a soil particle in the vertical direction. A seventh-order polynomial was generated based on these data points and was plotted in the line connected with circles. The portion of the curve between time 0 to time $5\Delta t$ is plotted at an enlarged scale in fig. 8b. The horizontal line was actually approximated by an oscillating curve with the difference less than 0.023 mm. When the derivatives of the polynomial were taken at various times, however, the values were not zero. As a result, nonzero velocities or nonzero strain rates existed in this time interval. In other words, positive deformation energy was computed in the portion of the soil in which measured soil movements were actually zero. The deformation energy was always positive because the components of the strain rate tensor in equation 9 were squared before summing for every small soil volume. In some cases, when the soil particles were undergoing rigid-body movements, i.e. the soil particles moved at constant velocity without interval energy dissipation, positive deformation energy would be computed for the same reason described above.

Among all these reasons, it is believed that the errors caused by high-order polynomial approximations were most serious. To overcome this difficulty, the computer program can be modified as described below.

65. The measured displacements should be smoothed before being fed into the computer. (The dashed line in fig. 8a is a smoothed displacement-time curve.) In the time interval between zero and $5\Delta t$, the velocities would be assumed equal to zero. A polynomial with very low order or a simple function would be accurate enough to approximate this displacement-time curve without oscillation. It should be pointed out that the soil displacemnts were actually very small, the differences between the smooth curve and actual measurements were less than 1 mm. In fact, measurements less than 1 mm were determined quite arbitrarily. It is reasonable to believe that the smoothed curve would better represent the real displacement-time relations of the soil particles, since the soil sample could be considered a continuous medium.

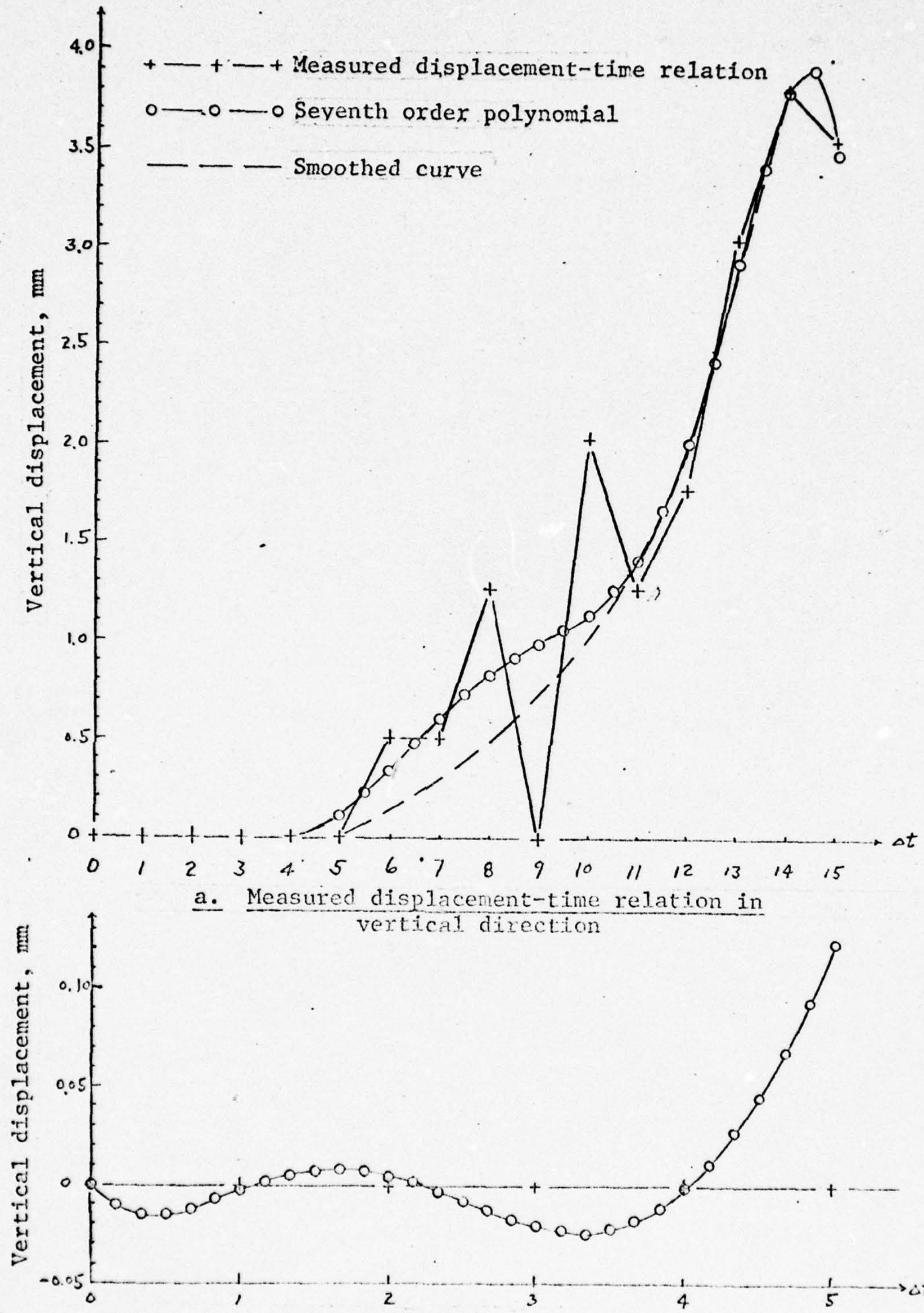

a. Measured displacement-time relation in vertical direction

b. Enlarged portion of a above

Fig. 8. Displacement-time curves

Conclusions

66. Based on the test data and computer results, it is concluded that:

a. The soil patterns under penetration can be drawn based on the measured soil particle movements (paragraphs 50-59).

b. The soil flow patterns in two-dimensional, plane strain cases are different from those in axisymmetric cases. In both cases, the shape of the stream (or flow) lines change with change in penetration speeds. In general, at the high penetration speeds of this study, the rate of change in the slope of the stream lines is greater and the distances from the ends of the stream lines to the probe become smaller than at slow speeds. Also, at the high penetration speeds, the rate of velocity change (or strain rate) along stream lines is greater; stresses in the soil are consequently greater to counterbalance the higher penetration force (paragraph 53).

c. The clay beneath the moving probe does not move entirely as a rigid body along a unique failure surface; rather it moves along infinite numbers of failure surfaces (paragraph 54).

d. The penetration resistances computed from measured soil movements are larger than measured values, indicating the possibility that the soil constant determined from triaxial tests may not represent the real soil strength under penetration (paragraphs 62 and 63).

e. The apparent discrepancy between computed and measured penetration resistance suggests that the usual mathematical procedure, which tends to magnify the errors inherent in the basic test data, is not appropriate for the problem of soil-vehicle interaction, unless an objective method to smooth the experimental curves is developed (paragraphs 64 and 65).

Literature Cited

1. Christian, J. T., "Two-Dimensional Analysis of Stress and Strain in Soils; Plane-Strain Deformation Analysis of Soil," Contract Report No. 3-129, Report 3, Dec 1966, U. S. Army Engineer Waterways Experiment Station, CE, Vicksburg, Miss.

2. Drucker, D. C., "A More Fundamental Approach to Plastic Stress-Strain Relations," Proceedings, First U. S. National Congress on Applied Mechanics, 1951, pp 487-491.

3. Drucker, D. C. and Prager, W., "Soil Mechanics and Plastic Analyses or Limit Design," Quarterly of Applied Mathematics, Vol 10, 1952, pp 157-175.

4. Drucker, D. C., Gibson, R. E., and Henkel, P. I., "Soil Mechanics and Work-Hardening Theories of Plasticity," Transactions, American Society of Civil Engineers, Vol 122, 1957, pp 338-346.

5. Jumikis, A. R., Mechanics of Soils, Van Nostrand, Princeton, N. J., 1964, p 14.

6. Miller, P. M., "A Report on the Application of the Visioplasticity Method to Soft-Soil Mobility Problems," Technical Memorandum No. VJ-2330-G-53, 1968, Cornell Aeronautical Laboratory, Inc., Buffalo, N. Y.

7. Prager, W. and Hodge, P. G., Theory of Perfectly Plastic Solids, Wiley, N. Y., 1951, p 143.

8. Smith, J. L., "Strength-Moisture-Density Relations of Fine-Grained Soils in Vehicle Mobility Research," Technical Report No. 3-639, Jan 1964, U. S. Army Engineer Waterways Experiment Station, CE, Vicksburg, Miss.

9. Whitman, R. V., "Multidimensional Analysis of Stress and Strain in Soils," DASA No. 1558, 1964, Defense Atomic Support Agency, Washington, D. C.; prepared by Stanford Research Institute, Menlo Park, Calif.

10. Yong, R. N. and Webb, G. L., "Energy Considerations in Wheel-Clay Soil Interaction," Report No. DR EO 32 (Geophysics), June 1969, Soil Mechanics Series, McGill University, Montreal, Canada.

11. Zadnek, S., "The Slip Lines and Slip Surfaces in the Theory of Plasticity and Soil Mechanics," Applied Mechanics Review, Vol 15, 1961, p 753.

Table 1

Laboratory Soil Sample Data

Test No.	Penetrometer Type	Penetrometer Speed cm/sec	Moisture Content %	Saturation %	Resistance Total N	Resistance Unit kN/m^2
1	5.1-cm circular plate	0.004	49.1	97.5	110	54.2
2	5.4-cm circular cone	0.004	50.6	97.5	133	57.6
3	3.8- by 22.8-cm plate	0.004	51.7	99.0	350	40.2
4	5.1- by 25.4-cm plate	0.004	49.5	97.0	501	38.8
5	5.1- by 25.4-cm plate	3.0	49.7	99.0	750	58.6
6	5.1-cm circular plate	0.9	50.8	99.0	120	59.2
7	5.1-cm circular plate	3.0	49.9	97.5	140	68.9
8	5.1-cm circular plate	5.6	51.2	97.0	240	118.5
9	5.4-cm circular cone	0.9	51.8	99.0	160	68.9
10	5.4-cm circular cone	5.6	50.0	97.0	300	129.5

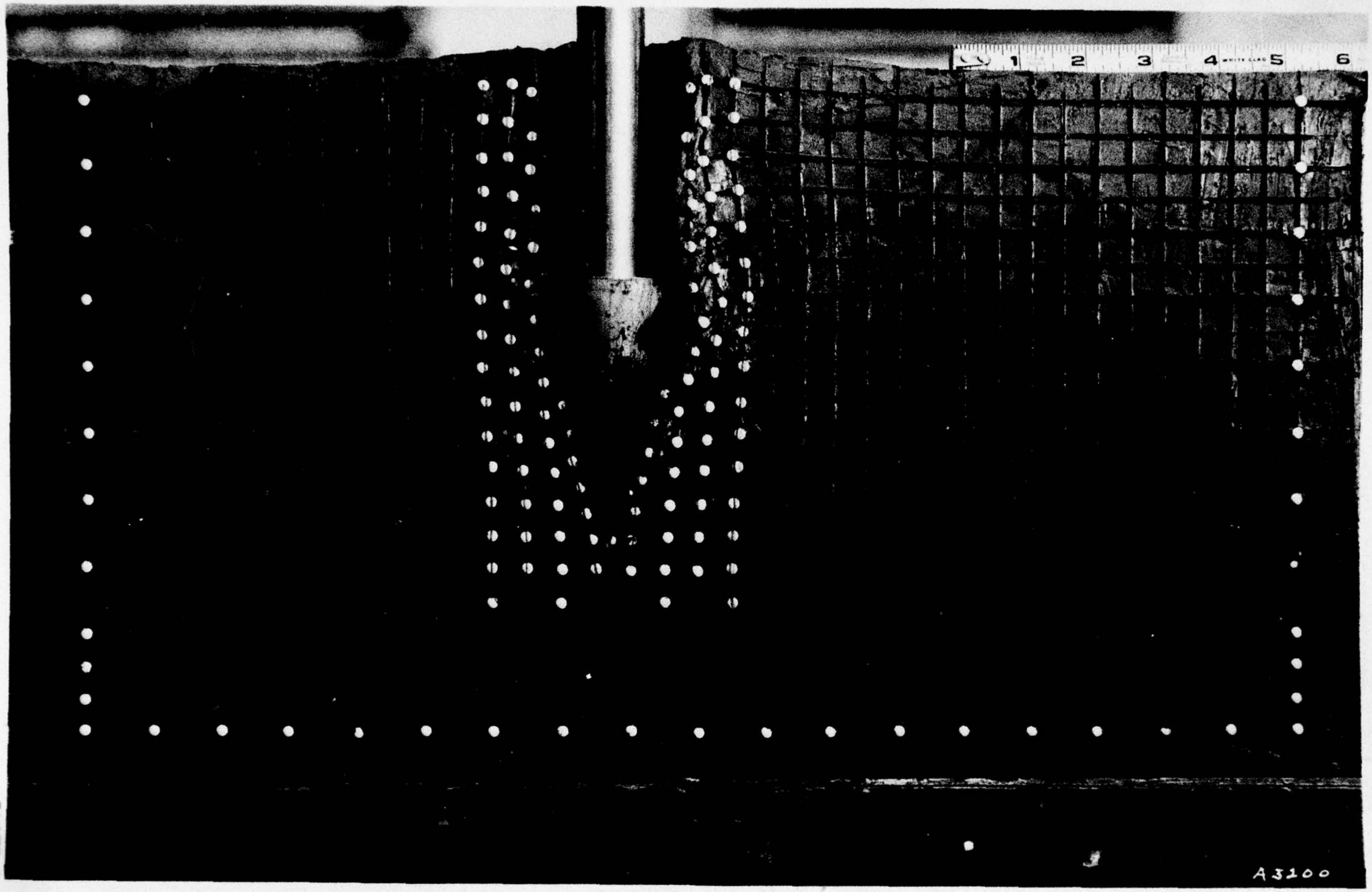

SOIL FLOW PATTERN AFTER PENETRATION OF 5.4-CM CIRCULAR CONE AT SPEED OF 5.6 CM/SEC

PLATE 1

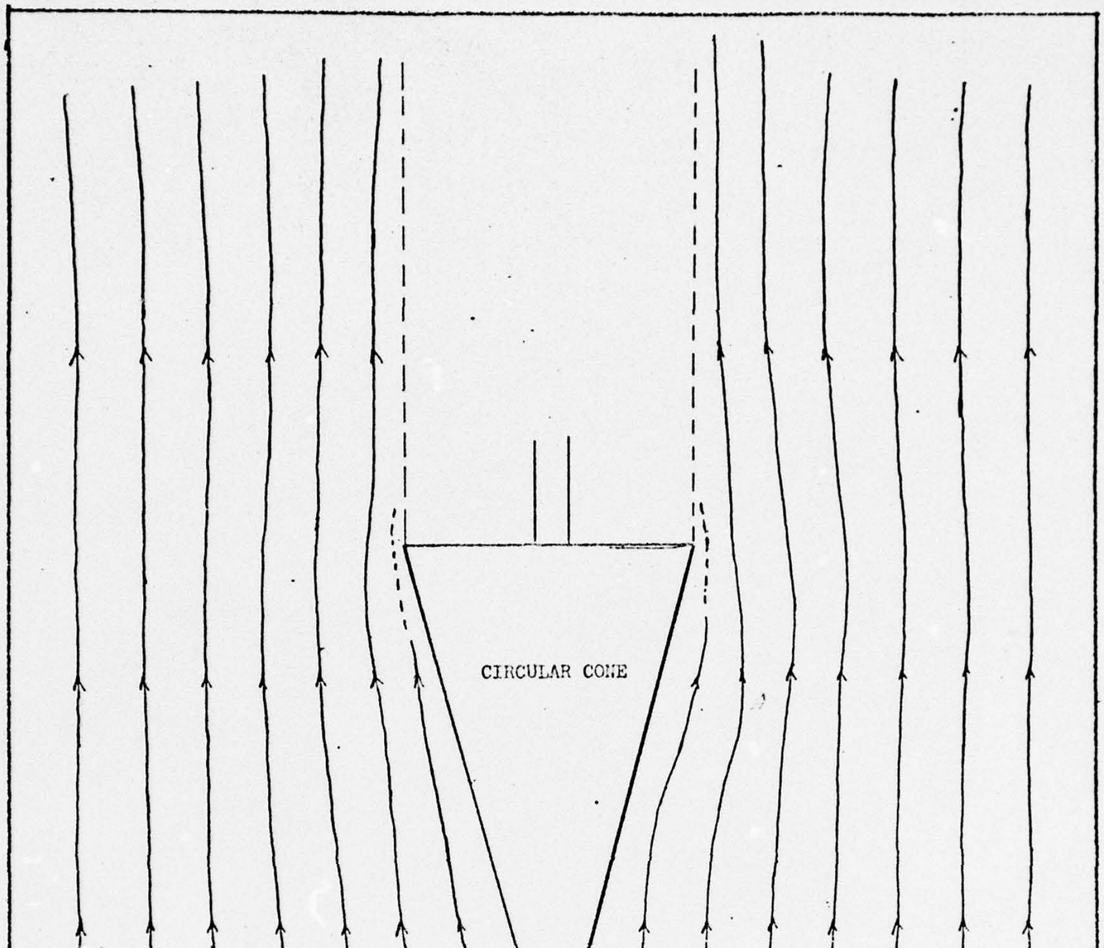

STREAM LINES OF SOIL PARTICLES AROUND A 5.4-CM CIRCULAR CONE; PENETRATION SPEED: 5.6 CM/SEC

PLATE 2

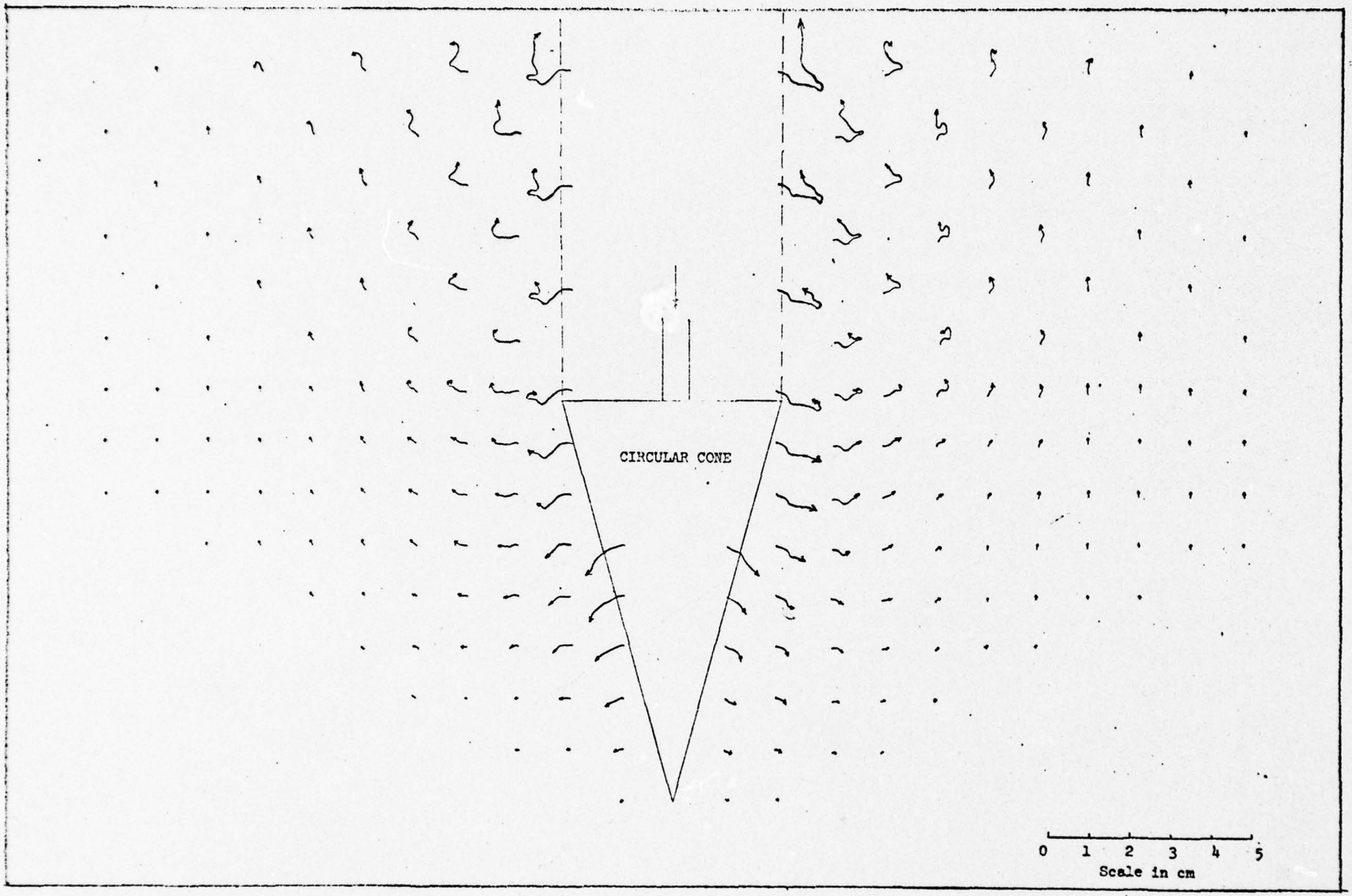

SOIL PARTICLE MOVEMENT AROUND A 5.4-CM CIRCULAR CONE; PENETRATION SPEED: 5.6 CM/SEC

PLATE 3

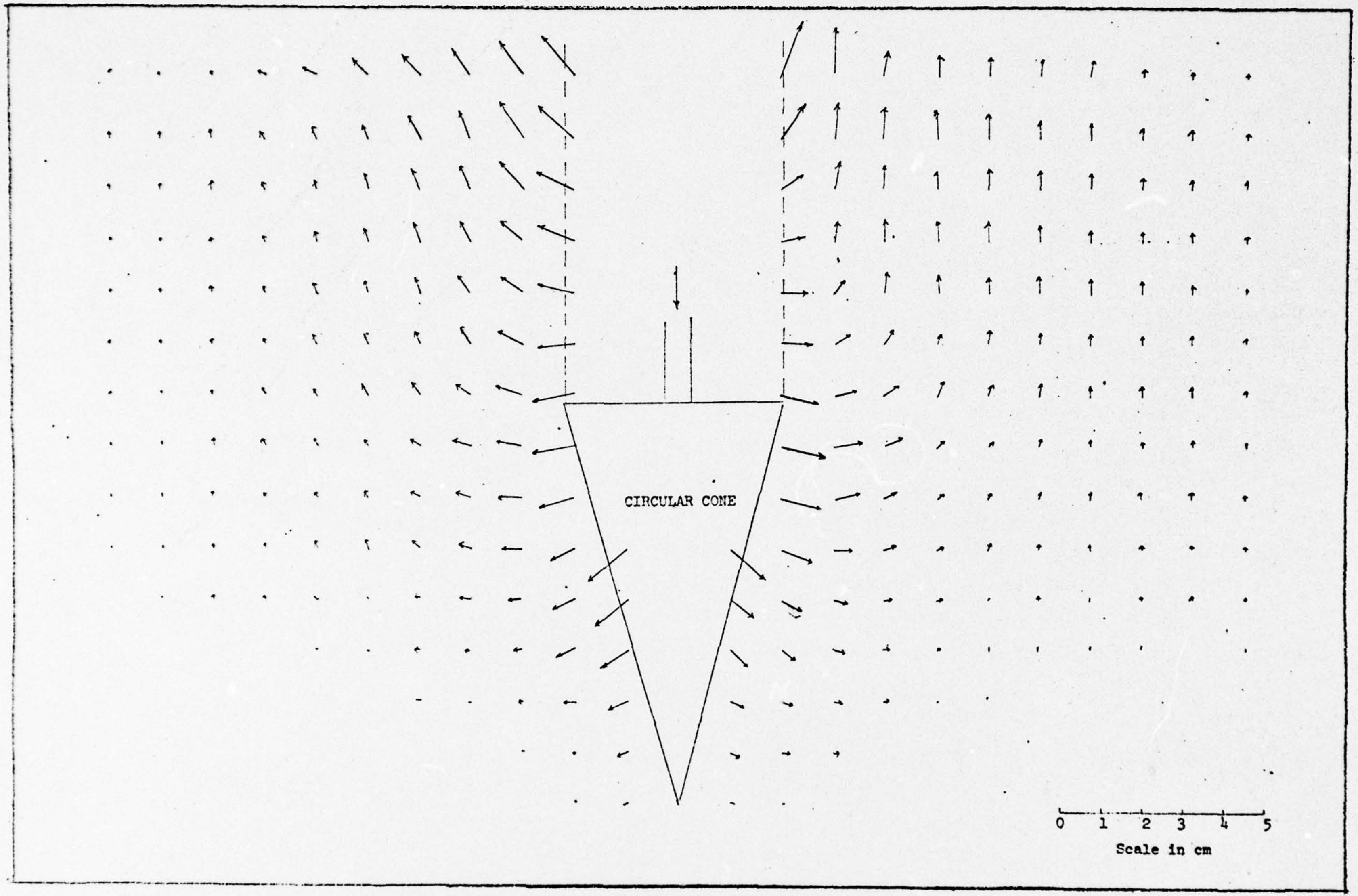

DISPLACEMENT BENEATH A 5.4-CM CIRCULAR CONE; PENETRATION SPEED: 5.6 CM/SEC

PLATE 4

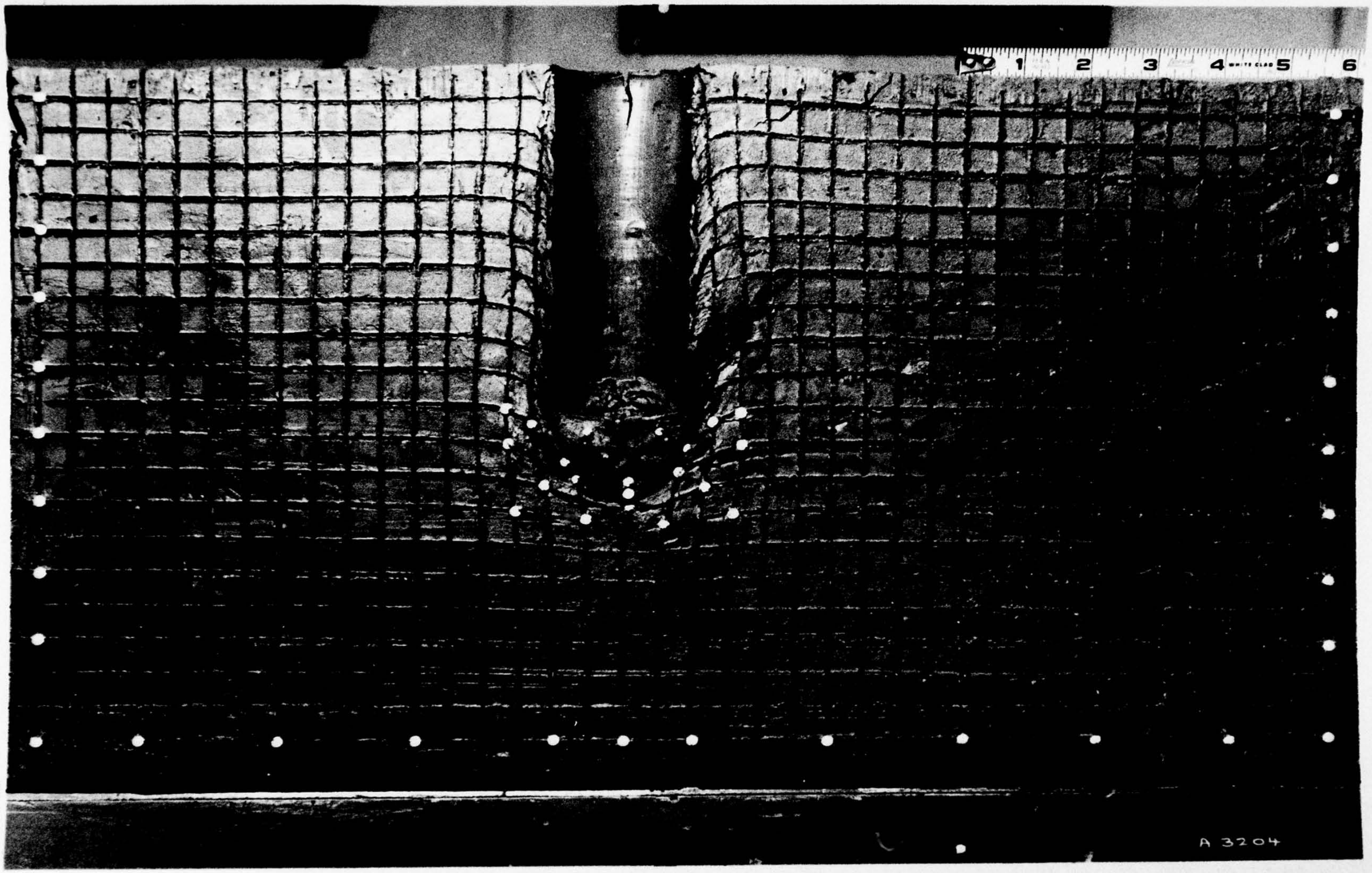

SOIL FLOW PATTERN AFTER PENETRATION OF 5.1-CM CIRCULAR PLATE AT SPEED OF 0.004 CM/SEC

PLATE 5

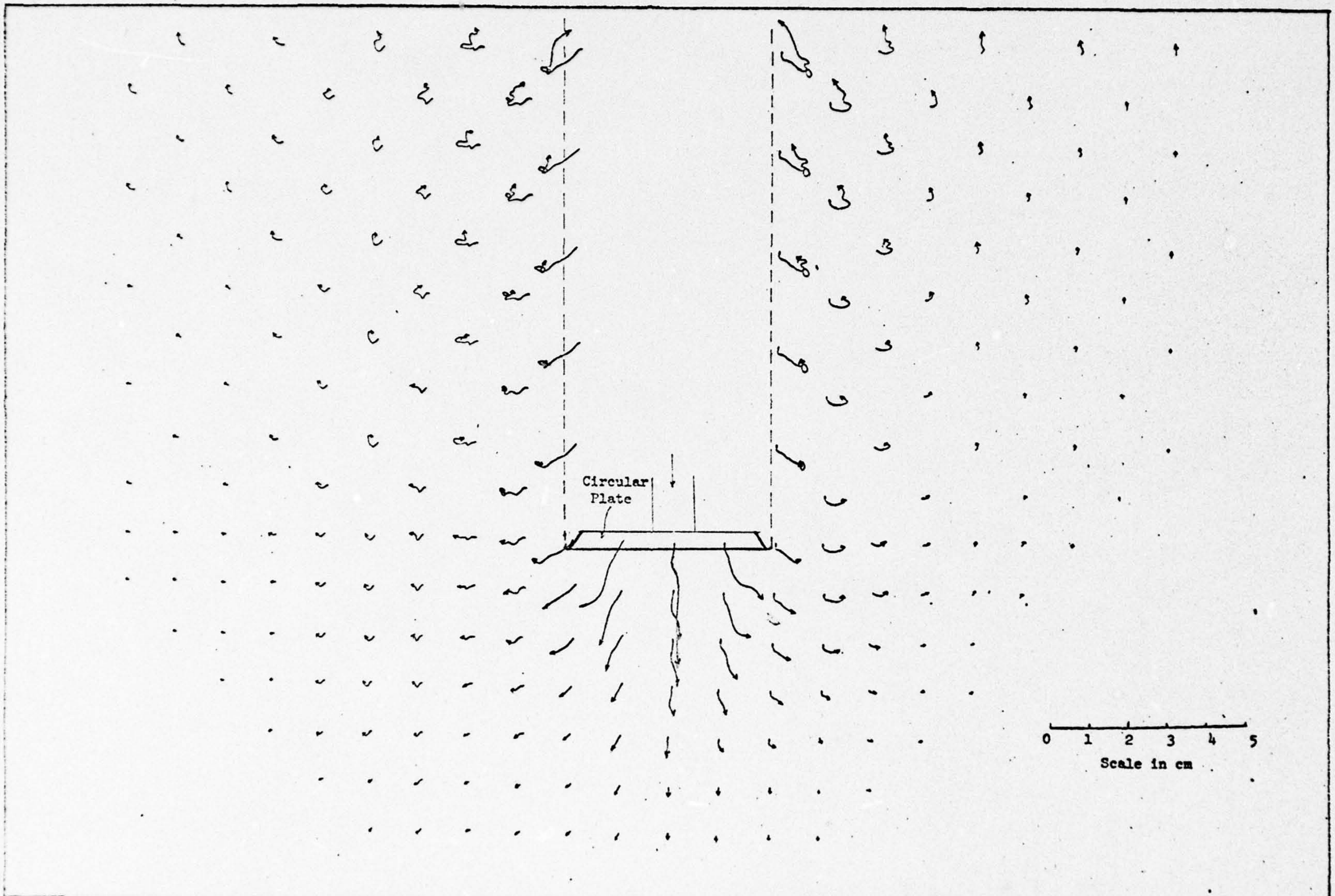

SOIL PARTICLE MOVEMENT AROUND A 5.1-CM CIRCULAR PLATE; PENETRATION SPEED: 0.004 CM/SEC

PLATE 6

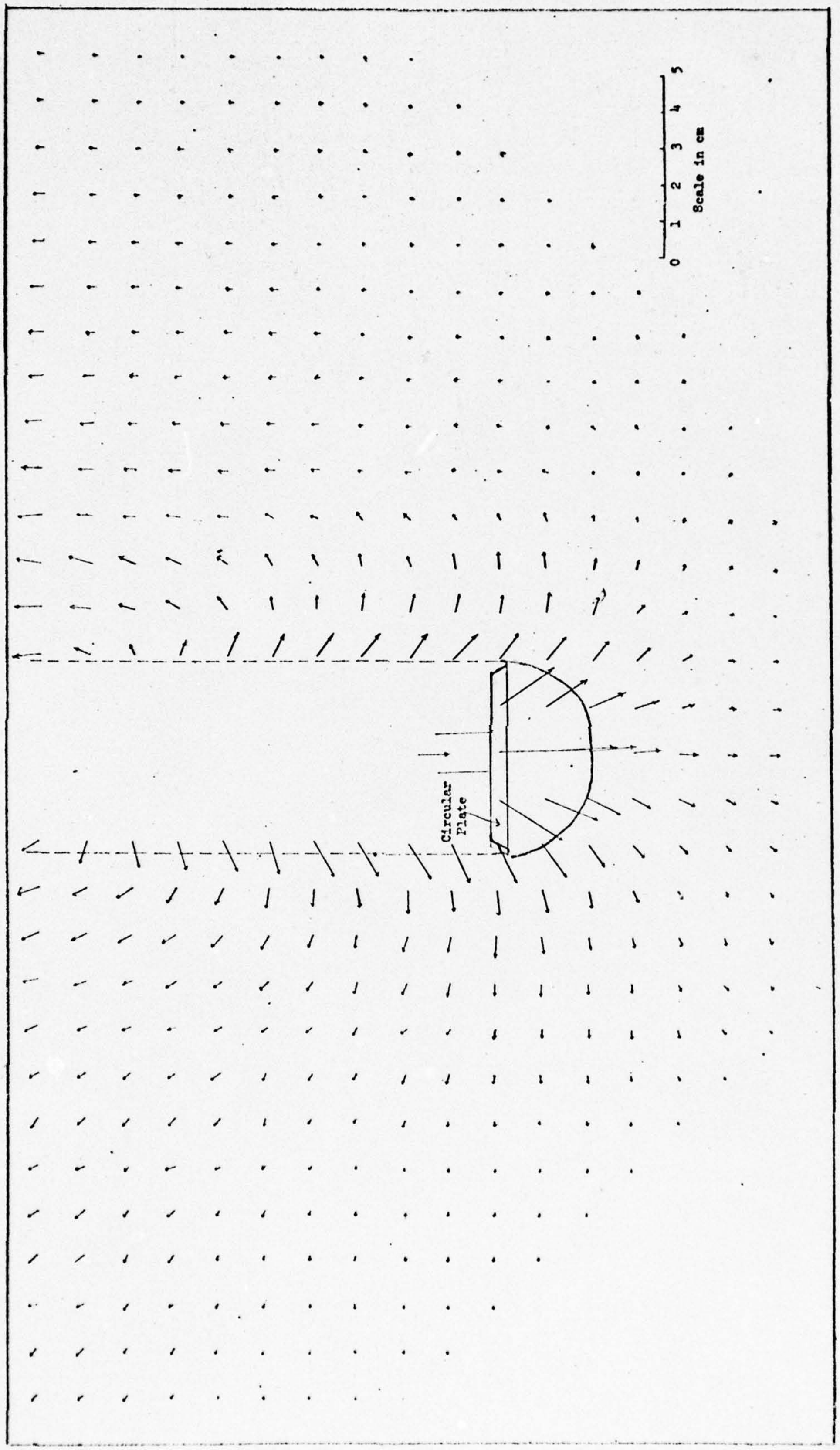

DISPLACEMENT BENEATH A 5.1-CM CIRCULAR PLATE; PENETRATION SPEED: 0.004 CM/SEC

PLATE 7

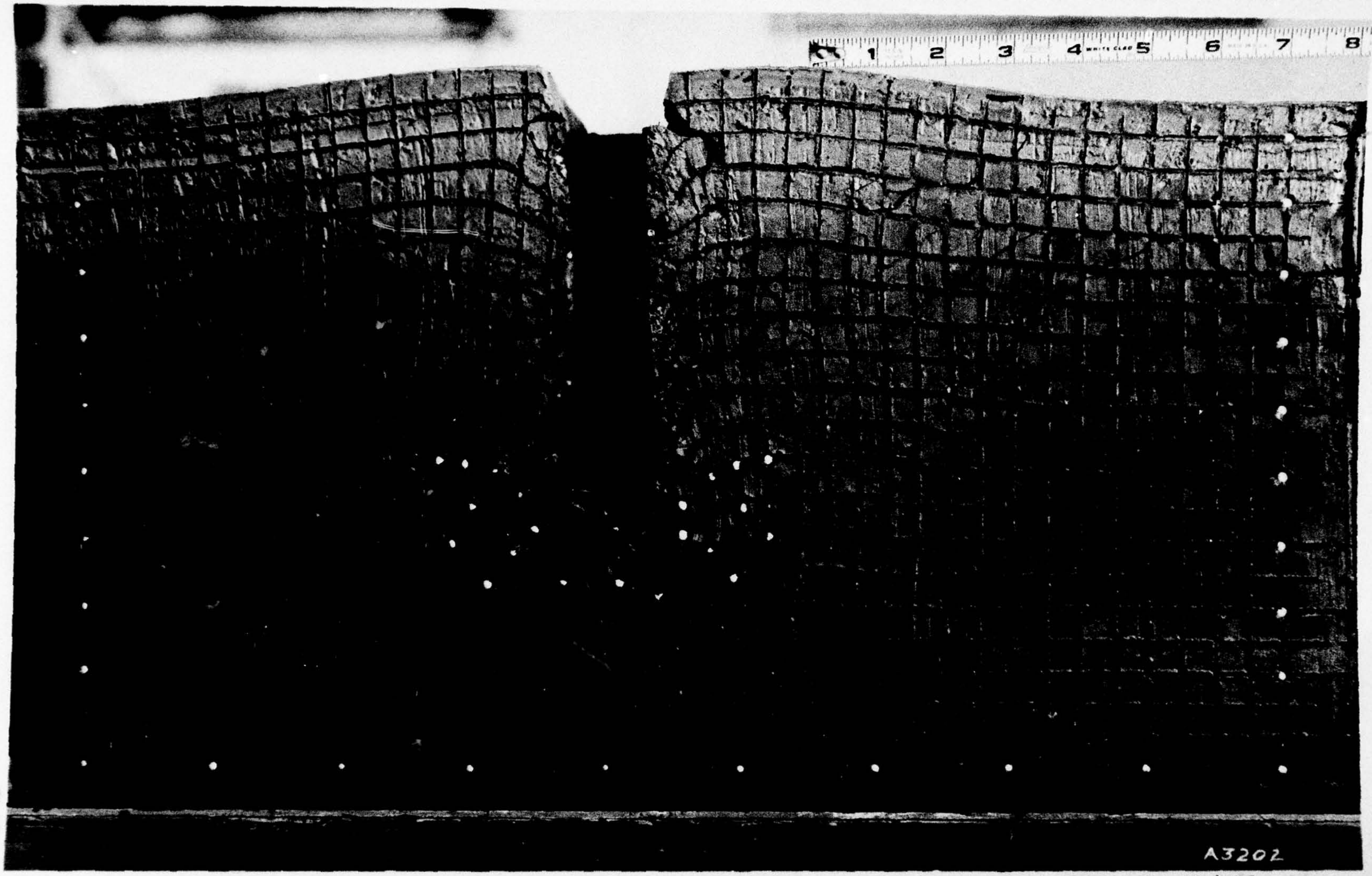

SOIL FLOW PATTERN AFTER PENETRATION OF 3.8- BY 22.8-CM RECTANGULAR PLATE AT SPEED OF 0.004 CM/SEC

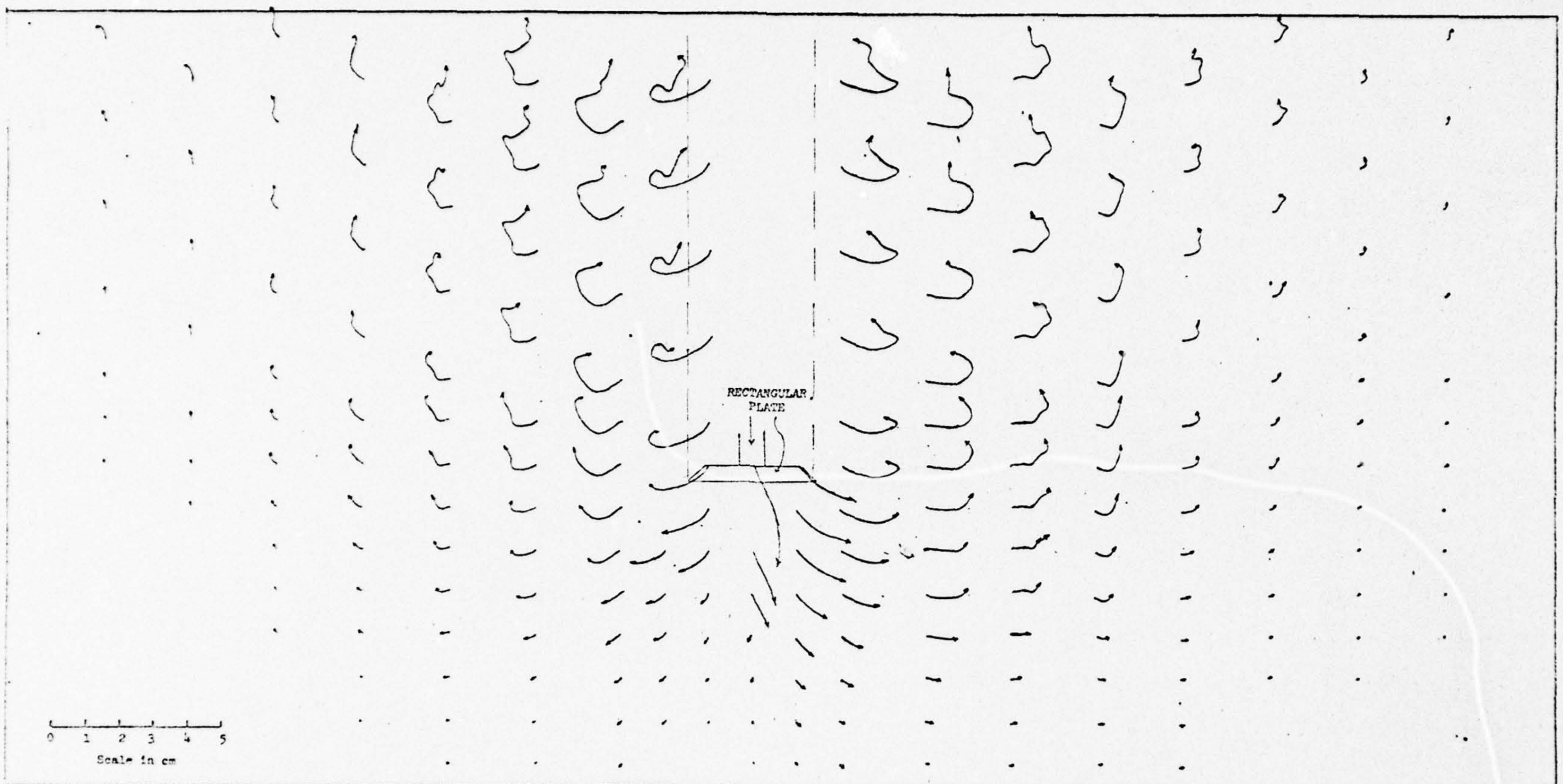

SOIL PARTICLE MOVEMENT AROUND A 3.8- BY 22.8-CM RECTANGULAR PLATE; PENETRATION SPEED: 0.004 CM/SEC

PLATE 9

PLATE 10

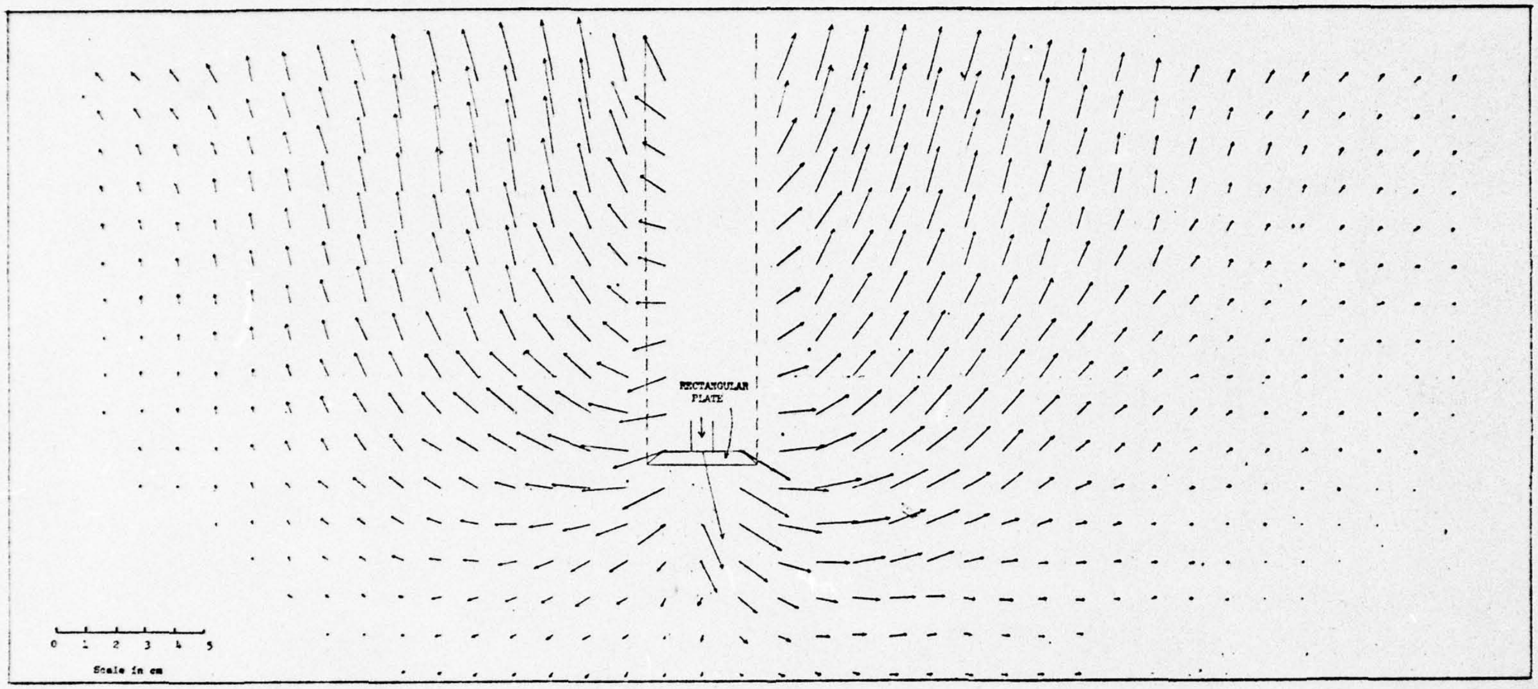

DISPLACEMENT BENEATH A 3.8- BY 22.8-CM RECTANGULAR PLATE; PENETRATION SPEED: 0.004 CM/SEC

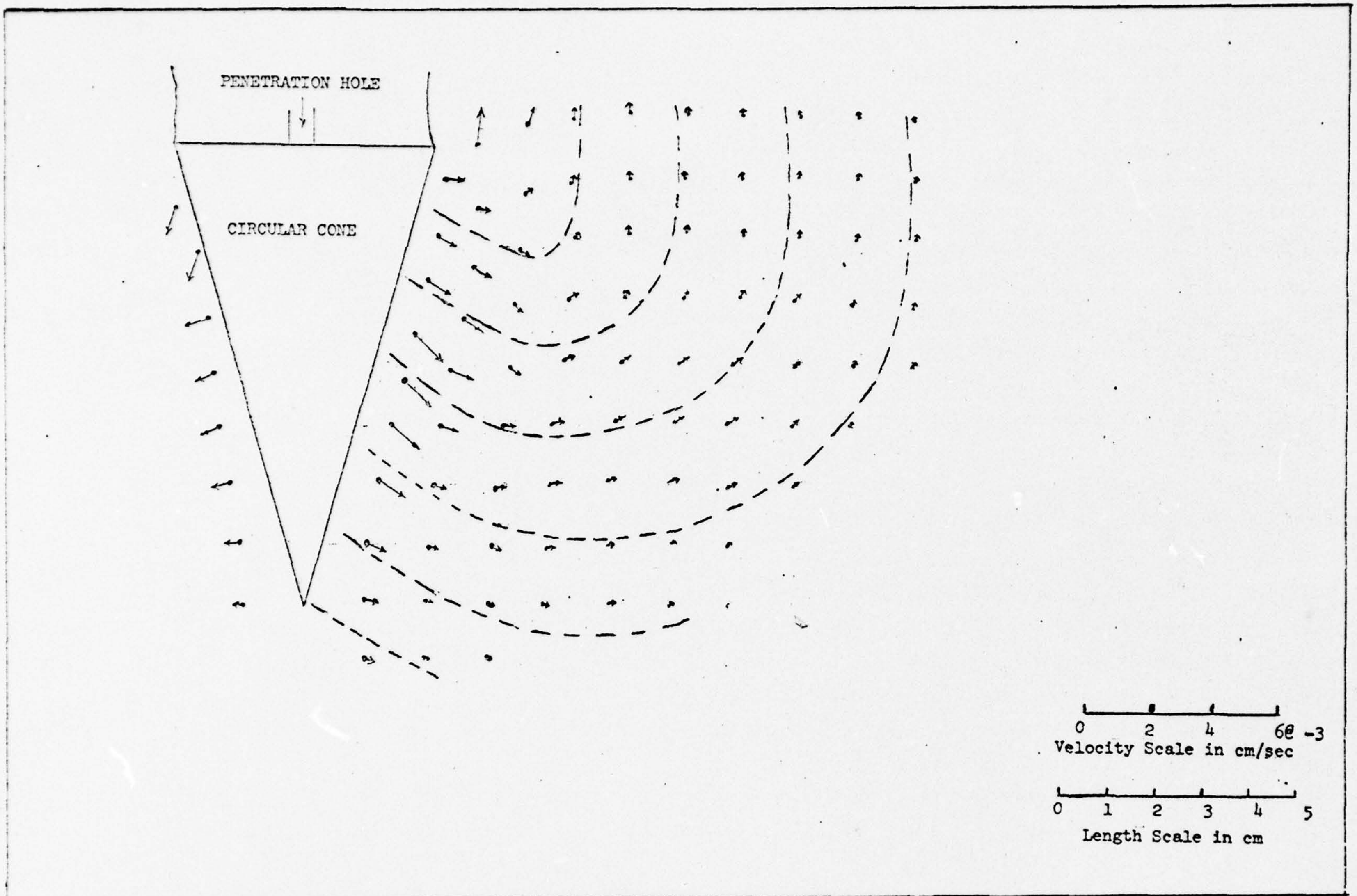

VELOCITY FIELD BENEATH A 5.4-CM CIRCULAR CONE; PENETRATION SPEED: 0.004 CM/SEC

PLATE 11

PLATE 12

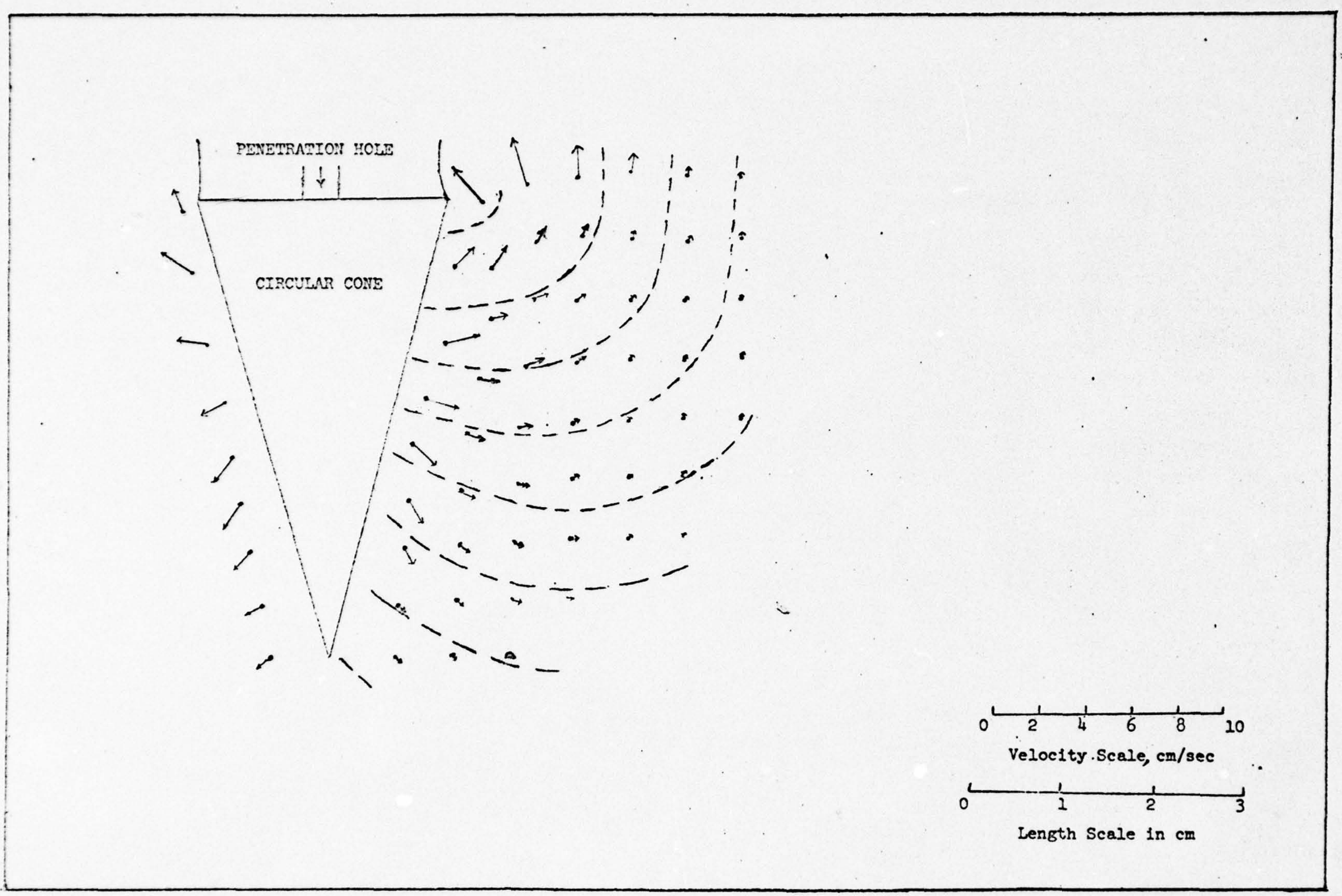

VELOCITY FIELD BENEATH A 5.4-CM CIRCULAR CONE; PENETRATION SPEED: 5.6 CM/SEC

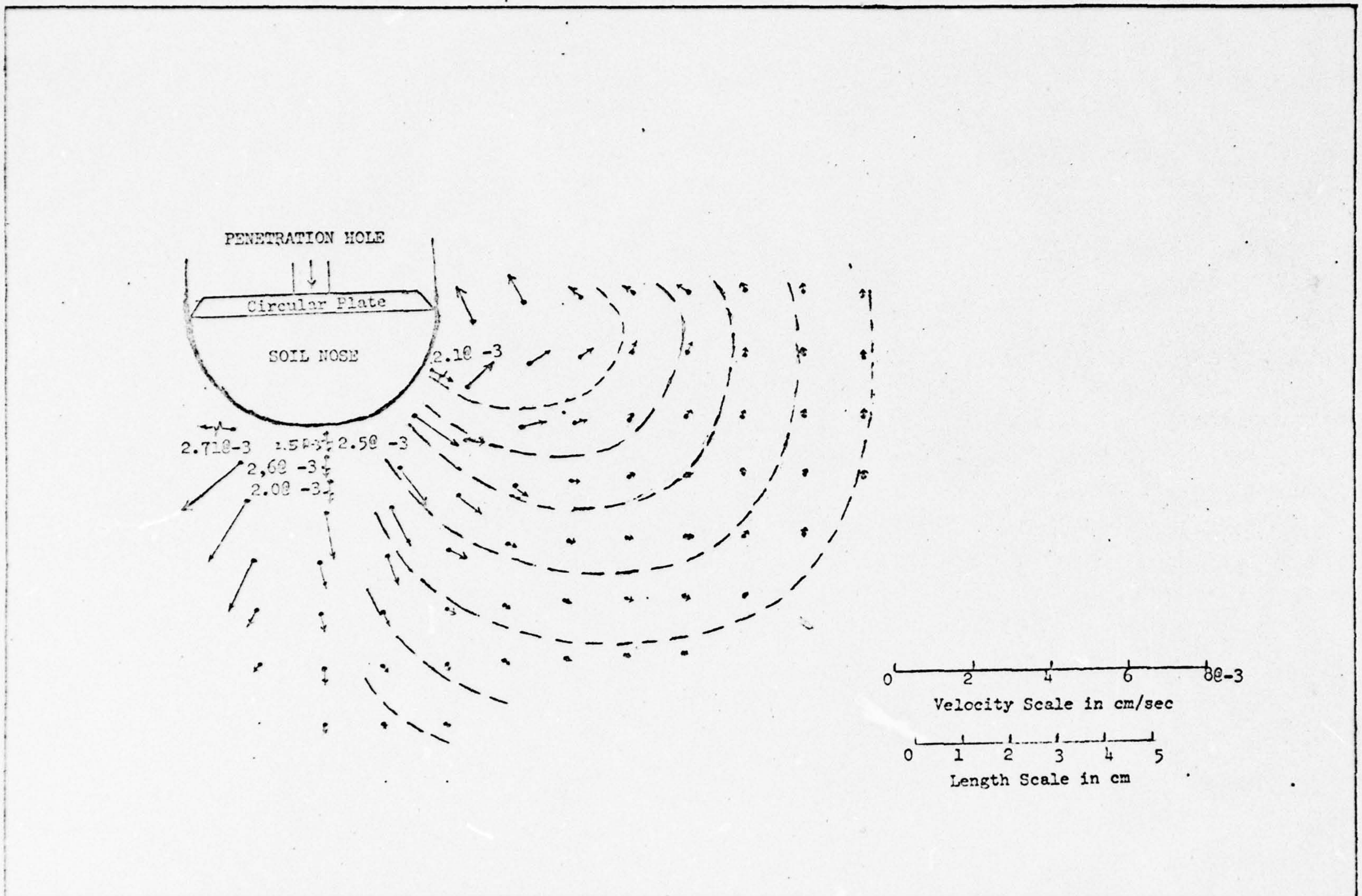

VELOCITY FIELD BENEATH A 5.1-CM CIRCULAR PLATE; PENETRATION SPEED: 0.004 CM/SEC

PLATE 13

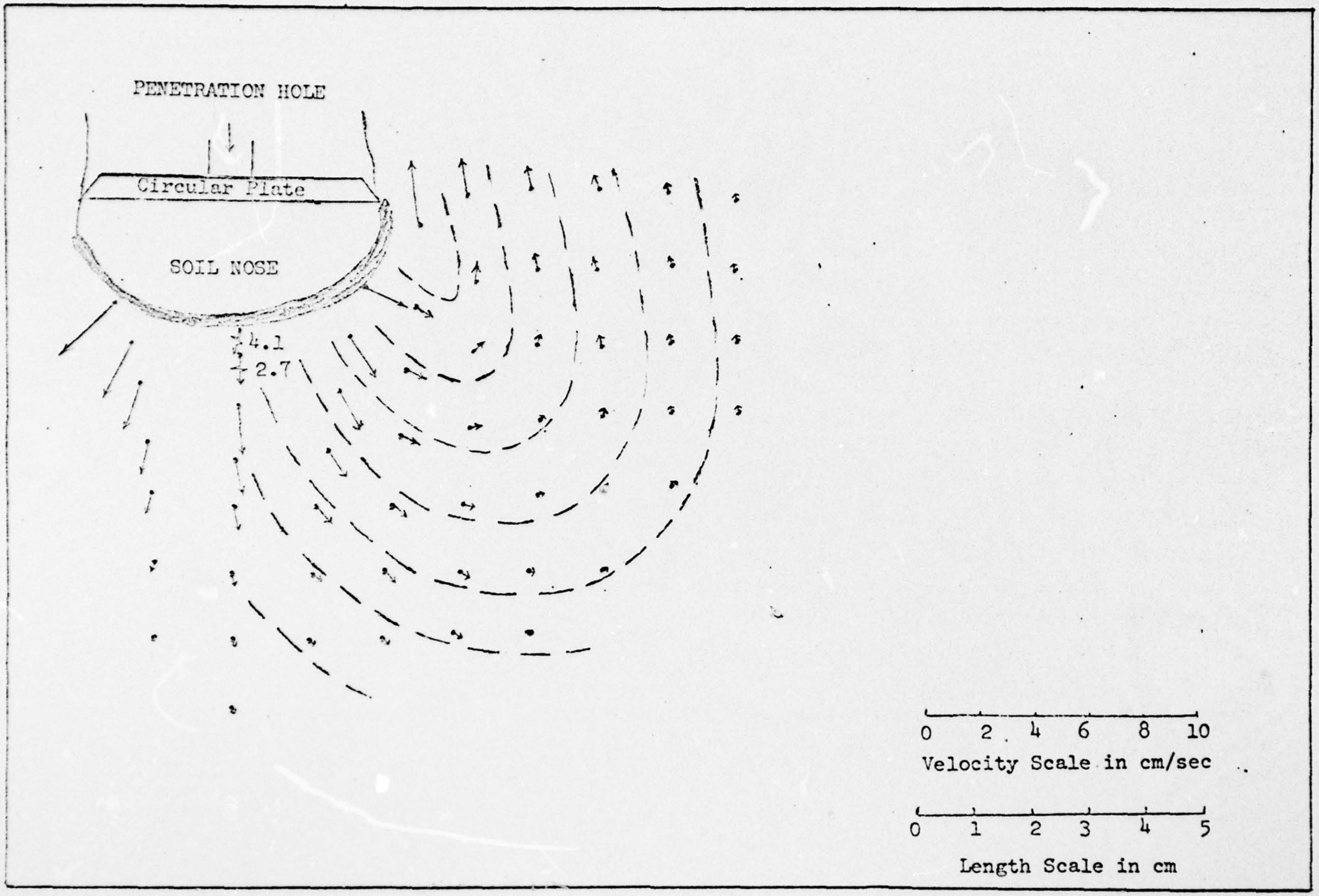

VELOCITY FIELD BENEATH A 5.1-CM CIRCULAR PLATE; PENETRATION SPEED: 5.6 CM/SEC

PLATE 14

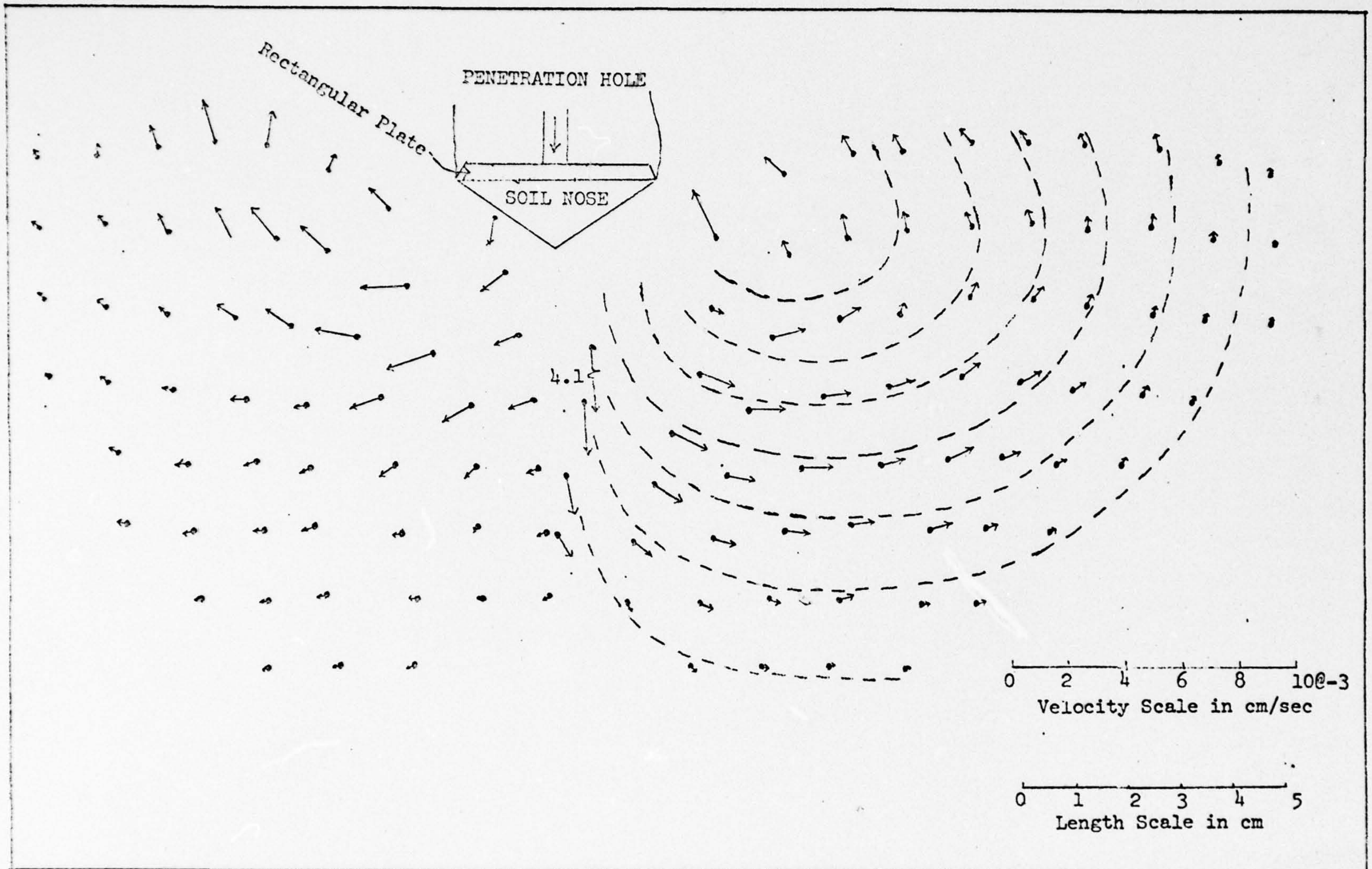

VELOCITY FIELD BENEATH A 3.8- BY 22.9-CM RECTANGULAR PLATE; PENETRATION SPEED: 0.004 CM/SEC

PLATE 15

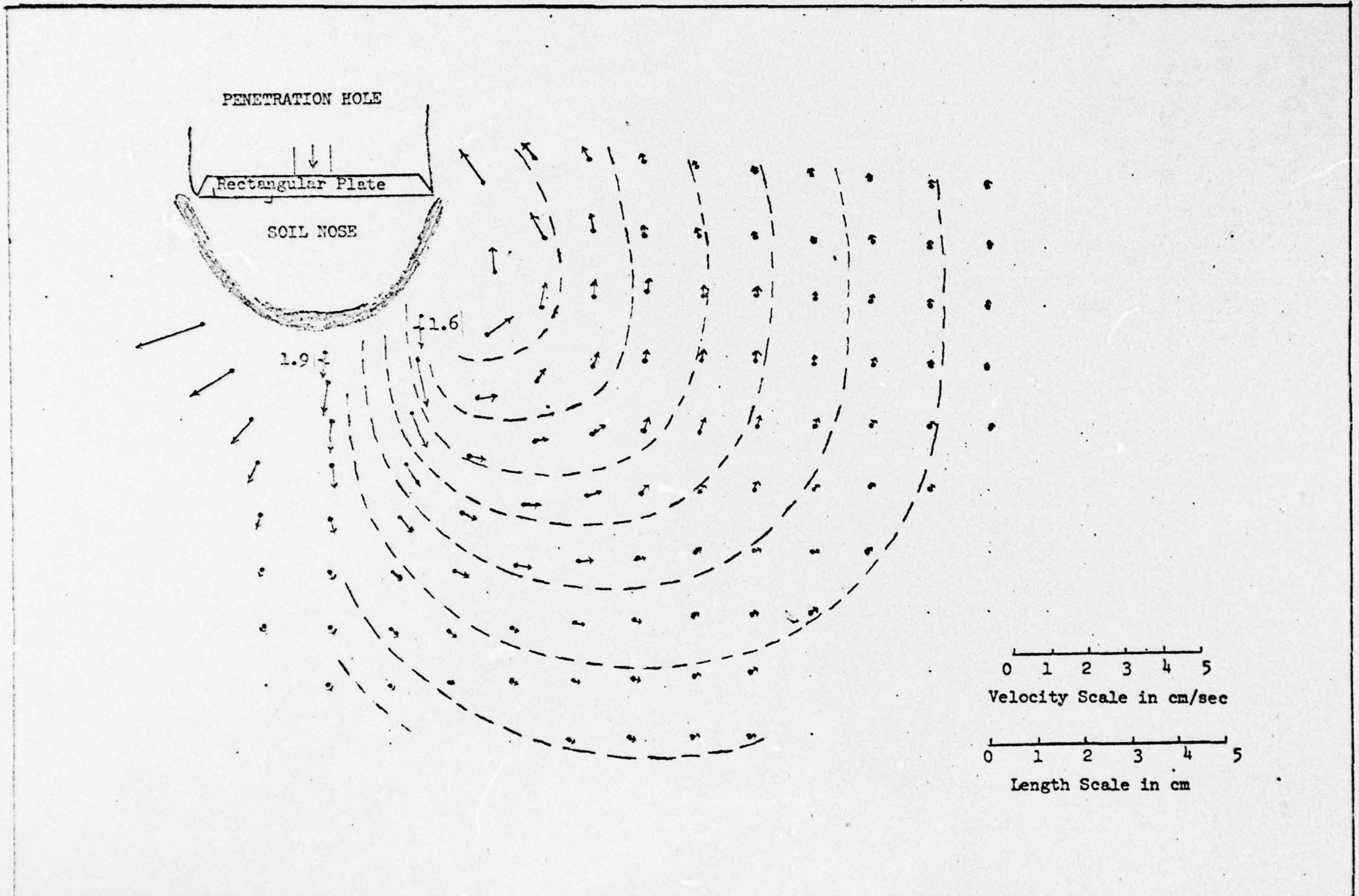

VELOCITY FIELD BENEATH A 5.1- BY 25.4-CM RECTANGULAR PLATE; PENETRATION SPEED: 3.1 CM/SEC

Appendix A: Computer Program


```
C              Y.T.CHOU   MOBILITY RESEARCH BRANCH,    W.E.S.
C          PURPOSE:COMPUTATION OF STRAIN RATE FIELD  IN THE SOIL MEDIUM.
       DIMENSION  R(21),Z(21),A1(9),A2(9),B2(9),A3(9),B3(9),A4(16),
      1B4(16),     A(9),B(9),VR1(21),VZ1(21),VR2(16,21),VZ2(16,21),VR(16,
      1            21),VZ(16,21),RR(16,21),CEDA(16,21),VEL(16,21),VRR(16,
      121),VRZ(16,21),VZR(16,21),VZZ(16,21),IP3(15),      ZA(15),TB(15),ZB(
      115),RA(15) ,YA(21),ZC(15),A5(16),B5(16) ,IP4(15)
       COMMON  X(21),Y(21),C(16),M,IP,LP,NR,NR1,CHECK
       EQUIVALENCE (VZ2(16,21),VZ(16,21),VZZ(16,21)),  (VR2(16,21),VR(16,
      121)),  (RR(16,21),VEL(16,21),CEDA(16,21),VRZ(16,21)),  (ZA(15),
      1TB(15),ZB(15),RA(15),ZC(15))
             READ  9000,     JJ1
             DO    3000            JJ=1,JJ1
       PRINT 1020
  1020 FORMAT  (1H1,
      1          40X,48HPURPOSE:COMPUTATIONS OF SOIL STRAIN RATE FIELD  //)
       READ 1,N11,N12,N2A,N2B,N2C,K1,IP,LP,NR,NR1,RES,V,CONE1,CONE2,
      1        SHEAR1
     1 FORMAT (10I5,F5.1,F10.8,3F5.1)
       READ 9000, N2AA,N2BB,NSAVE,NSAVEA,NSAVEE,NO1,NO2,NO3,NO4,NHA,NHB,
      1                NHC,NHD
       READ   9000,    NH1,NH2,NH3,NH4,NH5,NH6,NUMBER,IP1,IP2
  9000 FORMAT    (16I5 )
       READ     2001,   DIST1,DIST2,AREA1,AREA2,SQUARE
  2001 FORMAT    (8F10.5)
       IF (CONE1-1) 1001,1002,1003
  1001 IF (CONE2-1) 1004,1005,1005
  1004 PRINT 1010
  1010 FORMAT (20X,40HPROJECTOR:2 IN BY 10 IN SQUARE PLATE                )
       GO TO 1014
  1005 PRINT 1011
  1011 FORMAT (20X,45HPROJECTOR:1.5 IN BY 9 IN.SQUARE PLATE               )
       GO TO 1014
  1002 PRINT 1012
  1012 FORMAT (20X,45HPROJECTOR:2 IN CIRCULAR PLATE                       )
       GO TO 1014
  1003 PRINT 1013
  1013 FORMAT (20X,45HPROJECTOR:2 IN CIRCULAR CONE                        )
  1014 CONTINUE
       PRINT  1015 , V,NUMBER
  1015 FORMAT   (20X,29HPENETRATION SPEED(INCH/SEC.)=F10.8,10X,15HTEST
      1NUMBER=I5                                   )
       TINC=SQUARE/V
       SUM=0.
       DO      1000              J=1,2
       DO 81           M1=1,16
         DO 82           M2=1,21
        VR2(M1,M2)=0.
        VZ2(M1,M2)=0.
        RR(M1,M2)=0.
    82 CONTINUE
    81 CONTINUE
       DO    296     M3=1,21
       VR1(M3)=0.
```

```
      VZ1(M3)=0.
  296 CONTINUE
      IF (J-1)  1030,1030,1031
 1030 N1=N11
       NSAVEB=N01
      PRINT 212
  212 FORMAT (/9X,40H THE COMPUTED RESULTS ON THE RIGHT SIDE          )
      GO TO  1032
 1031 N1=N12
       NSAVEB=N02
      PRINT 214
  214 FORMAT (/9X,40H THE COMPUTED RESULTS ON THE LEFT  SIDE
 1032 CONTINUE
      READ 9000,    (IP3(I),I=NSAVE,NSAVEE)
      READ  9000,   (IP4(I),I=1,N1)
      DO        2               I1=1,N1
      IF (I1-2)      100,100,101
  100 IF (I1-1)      102,102,103
  102 N2=N2A
      N22=N2AA
      GO TO 104
  103 N2=N2B
      N22=N2BB
      GO TO 104
  101 N2=N2C
      N22=N2C
  104 READ  1044,    (R(I),I=1,N2)
      READ  1044,    (Z(I),I=1,N2)
 1044 FORMAT      (16F5.2)
      PRINT 5044,    I1
 5044 FORMAT (/24HTHE VALUES OF R AND Z IN I2,11HTH COLUMN      )
      PRINT 1044,    (R(I),I=1,N2)
      PRINT 1044,    (Z(I),I=1,N2)
      M=N2
       IF (I1-3)  9950,9951,9950
 9951 IP=IP1
       LP=IP
        GO TO 9954
 9950 IF (I1-4)                  9952,9953,9952
 9953 IP=IP1
        LP=IP
               GO TO 9954
 9952 IP=IP2
       LP=IP
 9954 CONTINUE
      DO      4                  I=1,N2
      X(I)=Z(I)
      Y(I)=R(I)
    4 CONTINUE
      IF (I1-5) 9500,9500,9501
 9500 CHECK=NHC
 9501 CONTINUE
      CALL LEAST
      LPP=LP+1
```

```
      DO     5                    I=1,LPP
    5 A1(I)=C(I)
      IF (I1-5)      1035,1035,1036
 1035 PRINT 1037,  (A1(I),I=1,LPP)
 1037 FORMAT    (10E12.5)
 1036 CONTINUE
      IF (J-1)      7006,7006,7002
 7006 IF (NH1)     7002,7002,7001
 7001 IF (I1-5)    7000,7000,7002
 7000 PRINT 7005
 7005 FORMAT (/35H CHECK STATION NUMBER ONE :1                 )
      ZZ=-0.5
      DO    7003                  I=1,15
      ZA(I)=ZZ+0.5
      RZ =A1(1)+A1(2)*ZA(I)+A1(3)*ZA(I)**2
      IF (LP-2)       60,60,61
   61 DO     62                  I2=3,LP
      IS  =I2+1
      TE1=A1(IS  )*ZA(I)**I2
      RZ=RZ+TE1
   62 CONTINUE
   60 CONTINUE
      PRINT  7004,   ZA(I),RZ
 7004 FORMAT  (2HZ=F5.2,40X,2HR=F10.5  )
      ZZ=ZA(I)
 7003 CONTINUE
 7002 CONTINUE
      DO        6                 I=2,N2
      SUB=I-1
      X(I)=SUB*TINC
       Y(I)=R(I)-R(1)
      YA(I)=Y(I)
      X(1)=0.
      Y(1)=0.
    6 CONTINUE
      CALL LEAST
      LPP=LP+1
      DO       7                 I=1,LPP
    7 A2(I)=C(I)
      Y(1)=0.
      R(1)=0.
      DO       8                  I=2,N2
      SUB=I-1
      Y(I)=SUB*0.5-Z(I)
    8 CONTINUE
      CHECK=NHC
      CALL LEAST
      LPP=LP+1
      DO       9                  I=1,LPP
    9 B2(I)=C(I)
      IF (J-1)        7015,7015,7010
 7015 IF (NH2)       7010,7010,7011
 7011 IF (I1-3)      7010,7012,7010
 7012 PRINT   7019
```

```
7019 FORMAT    (// 45H CHECK STATION NUMBER TWO :2    (U,W    )        )
     PRINT  9980,     (X(I),  I=1,N2)
     PRINT 9980,    (YA(I),I=1,N2)
     PRINT 9980,     (Y(I),I=1,N2)
9980 FORMAT    (12E10.3)
     TT=-TINC/2.
     DO      7013                 I=1,16
     TB(I)=TT +TINC/2.
     WA=B2(1)+B2(2)*TB(I)+B2(3)*TB(I)**2
     IF    (LP-2)       70,70,71
  71 DO       72                      I2=3,LP
     IRR =I2+1
     TE1=B2(IRR )*TB(I)**I2
     WA=WA+TE1
  72 CONTINUE
  70 CONTINUE
     PRINT  7014,    TB(I),WA
7014 FORMAT    (2HT=F5.2,40X,2HW=F10.4              )
     TT =TB(I)
7013 CONTINUE
7010 CONTINUE
     IF (NHA)       291,291,292
 292 PRINT 293,        J,I1
 293 FORMAT   (//60X,16HBRAIN WASH AT J=I2,5X, 6HCOLUMN I3, 8HU THEN W/)
     PRINT  9980,     (X(I),  I=1,N2)
     PRINT 9980,    (YA(I),I=1,N2)
     PRINT 9980,     (Y(I),I=1,N2)
 291 CONTINUE
     DO      10                   I=2,N2
     SUB=I-1
     VR1(I)=A2(2)+2.*A2(3)*TINC*SUB
     VZ1(I)=B2(2)+2.*B2(3)*TINC*SUB
     IF   (LP-2)     50,50,51
  51 DO  53                     I2=3,LP
     IQ1=I2-1
     IQ2=I2+1
     T=I2
     TE1=T*A2(IQ2)*(TINC*SUB)**IQ1
     TE2=T*B2(IQ2)*(TINC*SUB)**IQ1
     VR1(I)=VR1(I)+TE1
     VZ1(I)=VZ1(I)+TE2
  53 CONTINUE
  50 CONTINUE
  10 CONTINUE
     VR1(1)=0.
     VZ1(1)=0.
     DO      11                   I=1,N2
     X(I)=Z(I)
     Y(I)=VR1(I)
     YA(I)=Y(I)
  11 CONTINUE
     IF  (I1-1) 9502,9502,9503
9502 CHECK=NHC
9503 CONTINUE
```

```
      M=N2
      CALL   LEAST
      LPP=LP+1
      DO      12                     I=1,LPP
   12 A3(I)=C(I)
      IF (I1-1)  6000,6000,6001
 6000 PRINT  1037,    (A3(I),I=1,LPP)
 6001 CONTINUE
      DO      13                     I=1,N2
   13 Y(I)=V21(I)
      CALL   LEAST
      LPP=LP+1
      DO      14                     I=1,LPP
   14 B3(I)=C(I)
      IF (J-1)      7025,7025,7020
 7025 IF   (NH3)      7020,7020,7021
 7021 IF   (I1-3)     7020,7022,7020
 7022 PRINT   7029
 7029 FORMAT       (// 40H CHECK STATION NUMBER THREE:3 (VR VZ          )
      PRINT  9980,     (X(I),   I=1,N2)
      PRINT  9980,   (YA(I),I=1,N2)
      PRINT 9980,      (Y(I),I=1,N2)
      ZZ=-1.
      DO   7023                      I=1,10
      ZB(I)=ZZ+1.
      VV=B3(1)+B3(2)*ZB(I)+B3(3)*ZB(I)**2
      IF    (LP-2)    86,86,87
   87 DO  88                        I2=3,LP
      IQ1=I2+1
      TE1=B3( IQ1)*ZB(I)**I2
      VV=VV+TE1
   88 CONTINUE
   86 CONTINUE
      PRINT    7024,  ZB(I),VV
 7024 FORMAT  (2HZ=F5.2,40X,24HVELOCITY IN Z DIRECTION=F14.8            )
      ZZ=ZB(I)
 7023 CONTINUE
 7020 CONTINUE
      IF (NHB) 294,294,7085
 7085 PRINT    7086,   J,I1
 7086 FORMAT  (//60X,16HBRAIN WASH AT J=I2,5X, 6HCOLUMN I3,9HVR AND VZ/)
      PRINT  9980,     (X(I),   I=1,N2)
      PRINT 9980,    (YA(I),I=1,N2)
      PRINT 9980,     (Y(I),I=1,N2)
  294 CONTINUE
      DO       15                   I2=NSAVE,N22
      SUB=I2-1
      VR2(I1,I2)=A3(1)+A3(2)*SUB*0.5+A3(3)*((SUB*0.5)**2)
      VZ2(I1,I2)=B3(1)+B3(2)*SUB*0.5+B3(3)*((SUB*0.5)**2)
      RR(I1,I2 )=A1(1)+A1(2)*SUB*0.5+A1(3)*((SUB*0.5)**2)
      IF    (LP-2)    90,90,91
   91 DO  92                        I=3,LP
       IQ1=I+1
      TE1=A3( IQ1)*(SUB*0.5)**I
```

```
      TE2=B3( IQ1)*(SUB*0,5)**I
      TE3=A1(IQ1)*(SUB*0,5)**I
      VR2(I1,I2)=VR2(I1,I2)+TE1
      VZ2(I1,I2)=VZ2(I1,I2)+TE2
      RR(I1,I2)=RR(I1,I2)+TE3
   92 CONTINUE
   90 CONTINUE
        IF (RR(1,I2)-0.0000001)    301,301,302
  301 RR(1,I2)=0.
  302 CONTINUE
   15 CONTINUE
        DO   4000       I=1,N22
          VR2(1,I)=VR2(2,I)
          VZ2(1,I)=VZ2(2,I)
 4000 CONTINUE
      IF (J-1)            7036,7036,7030
 7036 IF  (NH4)       7030,7030,7031
 7031 IF  (I1-3)      7032,7032,7030
 7032 PRINT   7039,    I1
 7039 FORMAT   (// 52H CHECK STATION NUMBER FOUR:4 THE RR DISTANCE IN
     1                  I5,20HTH COLUMN                                )
      PRINT   7035,  (RR(I1,I2) ,I2=NSAVE,N22 )
      PRINT   7035,  (VR2(I1,I2),I2=NSAVE,N22)
      PRINT   7035,  (VZ2(I1,I2),I2=NSAVE,N22)
 7035 FORMAT   (12E10.3)
 7030 CONTINUE
    2 CONTINUE
      PRINT  7073
 7073 FORMAT (40X,30H LOOP 2 PRINT OUT  COMPLETED                  ///)
      N2=NSAVEE
      DO        20                 I2=NSAVE,N2
        IP=IP3(I2)
          LP=IP
      IF (I2-N2AA)  200,200,201
  200 NA=1
      GO TO  202
  201 IF (I2-N2BB)  203,203,204
  203 NA=2
      GO TO  202
  204 NA=3
  202 CONTINUE
      M=N1-NA+1
      DO       21                  I1=NA,N1
      I=I1-(NA-1)
      X(I)=RR(I1,I2)
      Y(I)=VR2(I1,I2)
      YA(I)=Y(I)
   21 CONTINUE
      IF (I2-N2AA) 9505,9505,9504
 9505 CHECK=NHC
 9504 CONTINUE
      CALL   LEAST
      LPP=LP+1
      DO       22                  I=1,LPP
```

```
   22 A4(I)=C(I).
      IF (I2-N2AA)   6010,6011,6010
 6011 PRINT  1037,   (A4(I),I=1,LPP)
 6010 CONTINUE
      DO       23                 I1=NA,N1
      I=I1-(NA-1)
   23 Y(I)=VZ2(I1,I2)
      CHECK=NHC
      CALL   LEAST
      LPP=LP+1
      DO       24                 I=1,LPP
   24 B4(I)=C(I)
         IF (J-1)        7043,7043,7040
 7043 IF (NH5)     7040,7040,7041
 7041 IF (I2-N2AA)    305,305, 7040
  305 PRINT    7045,IP
 7045 FORMAT (//21HCHECK STATION NO.5:                        I3)
      PRINT    7046, I2
 7046 FORMAT (50H VELOCITY IN Z DIRECTION ALONG HORIZONTAL LINE I2=I2   )
      PRINT    7047.,  (VZ2(I1,I2), I1=1,N1  )
 7047 FORMAT  (12E10.3)
      PRINT    7048
 7048 FORMAT  (50H THE CORRESPONDING RR,THEN CORREPONDING VR AND VZ     )
      PRINT    7047 ,  (RR(I1,I2),  I1=1,N1  )
      PRINT  9980,     (X(I),  I=1,N1)
      PRINT 9980,     (YA(I),I=1,N1)
      PRINT 9980,     (Y(I),I=1,N1)
      RAA=-0.25
         DO       7050              I=1,16
      RA(I)=RAA+0.25
      VRA=A4(1)+A4(2)*RA(I)+A4(3)*RA(I)**2
      VZA=B4(1)+B4(2)*RA(I)+B4(3)*RA(I)**2
      IF   (LP-2)     95,95,96
   96 DO   97                     I1=3,LP
      IQ1=I1+1
      TE1=A4(IQ1)*RA(I)**I1
      TE2=B4(IQ1)*RA(I)**I1
      VRA=VRA+TE1
      VZA=VZA+TE2
   97 CONTINUE
   95 CONTINUE
      PRINT    7051,       RA(I),VRA,VZA
 7051 FORMAT  (2HR=F5.2,20X,4HVR= E12.5,20X,4HVZ=    E12.5)
      RAA=RA(I)
 7050 CONTINUE
 7040 CONTINUE
      DO       25                I1=NA,N1
      SUB=I1-1
      VR(I1,I2)=A4(1)+A4(2)*SUB*0.5+A4(3)*(SUB*0.5)**2
      VZ(I1,I2)=B4(1)+B4(2)*SUB*0.5+B4(3)*(SUB*0.5)**2
      IF (LP-2)      120,120,121
  121 DO     122                 I=3,LP
      IQ1= I+1
      TE1=A4(IQ1)*(SUB*0.5)**I
```

```
      TE2=B4(IQ1)*(SUB*0.5)**I
       VR(I1,I2)=VR(I1,I2)+TE1
       VZ(I1,I2)=VZ(I1,I2)+TE2
  122 CONTINUE
  120 CONTINUE
      VEL(I1,I2)=SQRT(VR(I1,I2)**2+VZ(I1,I2)**2)
   25 CONTINUE
      PRINT   26,     I2
   26 FORMAT  (/   48H THE COMPUTED VELOCITIES AT GRID POINTS ALONG
     1I3,44HTH ROW(COUNTED FROM THE BOTTOM OF THE MOLD)     )
      PRINT   9002,    (VEL(I1,I2),I1=1,N1)
 9002 FORMAT  (12E10.3)
      PRINT  9998
 9998 FORMAT  (10X,5HVZ:                    )
      PRINT  9002,    (VZ(I,I2),I=1,N1     )
      PRINT  9997
 9997 FORMAT  (10X,5HVR:                    )
      PRINT  9002,    (VR(I,I2),I=1,N1     )
      DO      27                   I1=NA,N1
   27 CEDA(I1,I2)=ATAN(VZ(I1,I2)/VR(I1,I2))*57.2
      PRINT   28
   28 FORMAT (43HTHE DEGREE OF ANGLE AT SAME ROW                  )
      PRINT   29,        (CEDA(I1,I2),I1=1,N1)
   29 FORMAT  (16F7.1)
      DO      30                   I1=NA,N1
      SUB=I1-1
      VRR(I1,I2)=A4(2)+2.*A4(3)*SUB*0.5
      VZR(I1,I2)=B4(2)+2.*B4(3)*SUB*0.5
      IF   (LP-2)      110,110,111
  111 DO  112                      I=3,LP
      IQ1=I+1
      IQ2=I-1
      T=I
      TE1=T*A4(IQ1)*(SUB*0.5)**IQ2
      TE2=T*B4(IQ1)*(SUB*0.5)**IQ2
      VRR(I1,I2)=VRR(I1,I2)+TE1
      VZR(I1,I2)=VZR(I1,I2)+TE2
  112 CONTINUE
  110 CONTINUE
   30 CONTINUE
  221 PRINT    222,   I2
  222 FORMAT (40H THE VALUES OF VRR AT GRID POINTS ALONG I3,6HTH ROW    )
      PRINT    223,   (VRR(I1,I2),I1=1,N1)
  223 FORMAT  (12E10.3)
      PRINT    224
  224 FORMAT (20H                   VZR                 )
      PRINT    223,   (VZR(I1,I2),I1=1,N1)
  220 CONTINUE
C
C
   20 CONTINUE
C
      PRINT    7071
 7071 FORMAT  (///10X,10HLOOP 20 OK              ///)
```

```
      DO      32                  I1=1,N1
         IP=IP4(I1)
         LP=IP
      IF    (I1-2)    230,230,231
  230 IF    (I1-1)    232,232,233
  232 N2=N2AA-N03
      GO TO  234
  233 N2=N2BB-N04
      GO TO  234
  231 N2=N2C
  234 M=N2-NSAVE+1
      DO      33                  I2=NSAVE,N2
      SUB=I2-1
      I6=I2-(NSAVE-1)
      X(I6)=SUB*0.5
      Y(I6)=VR(I1,I2)
   33 CONTINUE
      IF (I1-3)  9507,9507,9506
 9507 CHECK=NHC
 9506 CONTINUE
      CALL  LEAST
      LPP=LP+1
      DO      34                  I=1,LPP
   34 A5(I)=C(I)
      IF (I1-3)  6020,6021,6021
 6021      PRINT   1037,      (A5(I),   I=1,LPP)
 6020 CONTINUE
      DO      35                  I2=NSAVE,N2
      I6=I2-(NSAVE-1)
      Y(I6)=VZ(I1,I2)
   35 CONTINUE
      CALL   LEAST
      LPP=LP+1
      DO      36                  I=1,LPP
   36 B5(I)=C(I)
       IF   (I1-NSAVEB)      3011,3011,7060
 3011 IF (J-1)      7063,7063,7060
 7063 IF   (NH6)      7060,7060,7061
 7061 PRINT  7064,I1,IP
 7064 FORMAT (50H                  VR    AND    VZ      ALONG COLUMN
     1                    I3,I2         )
      PRINT  7062 , (VR(I1,I2), I2=1,N2C     )
      PRINT  7062 , (VZ(I1,I2), I2=1,N2C     )
 7062 FORMAT  (10E10.3 )
      ZZ=-0.75
      DO   3006               I=1,12
      ZC(I)=ZZ+0.75
      RZ1=A5(1)+A5(2)*ZC(I)+A5(3)*ZC(I)**2
           RZ2=B5(1)+B5(2)*ZC(I)+B5(3)*ZC(I)**2
      IF    (LP-2)         3007,3007,3008
 3008 DO     3009             I2=3,LP
      IS=I2+1
      TE1=A5(IS)    *ZC(I)**I2
      TE2=B5(IS)     *ZC(I)**I2
```

```
      RZ1=RZ1+TE1
      RZ2=RZ2+TE2
 3009 CONTINUE
 3007 CONTINUE
      PRINT    3010,  ZC(I),RZ1,RZ2
 3010 FORMAT   (E12.5,10X,E12.5,10X,E12.5)
      ZZ=ZC(I)
 3006 CONTINUE
 7060 CONTINUE
      DO       37                  I2=NSAVE,N2
      SUB=I2-1
      VRZ(I1,I2)=A5(2)+2.*A5(3)*SUB*0.5
      VZZ(I1,I2)=B5(2)+2.*B5(3)*SUB*0.5
      IF   (LP-2)     115,115,116
  116 DO  117                      I=3,LP
      IQ1=I-1
      IQ2=I+1
      T=1
      TE1=T*A5(IQ2)*(SUB*0.5)**IQ1
      TE2=T*B5(IQ2)*(SUB*0.5)**IQ1
      VRZ(I1,I2)=VRZ(I1,I2)+TE1
      VZZ(I1,I2)=VZZ(I1,I2)+TE2
  117 CONTINUE
  115 CONTINUE
   37 CONTINUE
      PRINT  6030, I1
 6030 FORMAT (26H VRZ AT GRID POINTS ALONG I3,11HTH COLUMNS              )
      PRINT    223,    (VRZ(I1,I2),I2=NSAVE,N2)
      PRINT    6031
 6031 FORMAT (20H                VZZ                 )
      PRINT    223,    (VZZ(I1,I2),I2=NSAVE,N2)
   32 CONTINUE
      PRINT       7072
 7072 FORMAT          (60X,10HLOOP 32 OK              ///)
      SUM2=0.
      DO          40               I1=1,NSAVEB
      IF(I1-2)    240,240,241
  240 IF(I1-1)    242,242,243
  242 N2=N2AA-N03
      AREA=AREA1
      DIST=DIST1
      GO TO  244
  243 N2=N2BB-N04
      SUB=I1-1
      DIST=0.5*SUB+DIST2
      AREA=AREA2
      GO TO  244
  241 N2=NSAVEE
      SUB=I1-1
      DIST=0.5*SUB+DIST2
      AREA=AREA2
  244 CONTINUE
      PRINT  130,     I1,NSAVEA
  130 FORMAT(/40X,24HTHE STRESS COMPONENTS IN I3,9HTH COLUMN  7H:NSAVE=
```

```
          1                           13                           )
            PRINT  131
        131 FORMAT (5X, 95HSR                                   SC                      SZ
          1              SRZ                                    J2         /)
            SUM1=0.
            IF (K1-1) 261,261,260
        260 DO      41               I2=NSAVEA,N2
            IF  (I2-N2)     3001,3002,3002
       3002 AREA=AREA/2.
       3001 CONTINUE
            ER=VRR(I1,I2)
            EC=VR(I1,I2)/DIST
            EZ=VZZ(I1,I2)
            GAMA=VRZ(I1,I2)+VZR(I1,I2)
            VA1=ER**2+EC**2+EZ**2
            VA2=1.+(GAMA**2/(VA1+GAMA**2))
            VA3=SQRT((0.5*VA1+0.25*GAMA**2)/(VA1**2))
            VA5=(0.5*VA1+0.25*GAMA**2)/(VA1**2)
            VA4=2.*3.14159*DIST*AREA*(VA2/VA5)*VA3
            SUM1=SUM1+VA4
            SR=1./SQRT(0.5*(1.+(EC**2/ER**2)+(EZ**2/ER**2))+0.25*(GAMA**2/ER**
           12))
            SC=1./SQRT(0.5*((ER**2/EC**2)+1.+(EZ**2/EC**2))+0.25*(GAMA**2/EC**
           12))
            SZ=1./SQRT(0.5*((ER**2/EZ**2)+(EC**2/EZ**2)+1.)+0.25*(GAMA**2/EZ**
           12))
            SRZ=1./SQRT(2.0*VA1/(GAMA**2)+1.00)
            WJ2=0.5*(SR**2+SC**2+SZ**2)+SRZ**2
            IF    (NHD)    41,41,2002
       2002 PRINT  132, SR,SC,SZ,SRZ,WJ2
        132 FORMAT (    E12.5,5X, E12.5,10X,E12.5, 7X,E12.5,18X,E12.5     )
         41 CONTINUE
            GO TO 275
        261 DO      42               I2=NSAVEA,N2
            IF (I2-N2)     3003,3004,3004
       3004 AREA=AREA/2.
       3003 CONTINUE
            ER=VRR(I1,I2)
            EZ=VZZ(I1,I2)
            GAMA=VRZ(I1,I2)+VZR(I1,I2)
            VA1=ER**2+EZ**2
            VA2=1.+(GAMA**2/(VA1+GAMA**2))
            VA3=SQRT((0.5*VA1+0.25*GAMA**2)/(VA1**2))
            VA5=(0.5*VA1+0.25*GAMA**2)/(VA1**2)
            VA4=AREA*(VA2/VA5)*VA3
            SUM1=SUM1+VA4
            SR     =1./SQRT(0.5*(1.+(EZ**2/ER**2))+0.25*(GAMA**2/ER**2))
            SC     =0.
            SZ     =1./SQRT(0.5*((ER**2/EZ**2)+1.)+0.25*(GAMA**2/EZ**2))
            SRZ=1./SQRT(2.0*VA1/(GAMA**2)+1.00)
            WJ2    =0.5*(SR     **2+SZ     **2)+SRZ     **2
            IF    (NHD)    42,42,2003
       2003 PRINT  273, SR,SC,SZ,SRZ,WJ2
        273 FORMAT (    E12.5,5X, E12.5,10X,E12.5, 7X,E12.5,18X,E12.5     )
```

```
   42 CONTINUE
  275 PRINT   43, I1,SUM1
   43 FORMAT  (  / 30X,10HTHE SUM OF I3,7HCOLUMN=E12.5            ///)
      SUM2=SUM2+SUM1
   40 CONTINUE
        IF (NHD)     2004,2004,2005
 2005 PRINT   45,    SUM2
   45 FORMAT  (32HTHE TOTAL SUM OF THIS HALF MOLD=E12.5        )
 2004 SUM=SUM+SUM2
 1000 CONTINUE
      ENE=RES*V
      PRINT   46,    RES,SUM,ENE
   46 FORMAT  (20X,30HTHE MEASURED RESISTANCE FORCE=F10.2  /
     1          20X,30HTHE COMPUTED ENERGY            =E12.5  /
     1          20X,26H COMPUTED R*V=                 E12.5/        )
 3000 CONTINUE
      CALL EXIT
      END
```

```
      SUBROUTINE  LEAST
      COMMON  X(21),Y(21),C(16),M,IP,LP,NR,NR1,CHECK
      DIMENSION  PIM1(50),PI(50),ALPHA(16),BETA(16),S(16),G(16),
     1           PERR(50),T(3)
      T(1)=2.8505852241
      T(2)=-2.0751480497E-03
      T(3)=-2.2520149609E-01
      ZER=0.
      ONE=1.
      IF (LP-IP) 104,106,106
  104 LP=IP
  106 N=LP+1
      K=IP+1
  120 DO 130   I=1,M
      PIM1(I)=ZER
      PI(I)=ONE
  130 CONTINUE
      DO  140  I=1,16
      S(I)=ZER
      BETA(I)=ZER
  140 ALPHA(I)=ZER
      A1=ZER
      B1=ZER
      WII=M
      I=1
  160 WI=ZER
      DO 170  L=1,M
  170 WI=WI+Y(L)*PI(L)
      S(I)=WI/WII
      IF (I-N) 180,302,302
  180 A1=ZER
      DO  190  L=1,M
  190 A1=A1+X(L)*PI(L)**2
      A1=A1/WII
      ALPHA(I+1)=A1
      WI=ZER
      DO  210 L=1,M
      PIP1=(X(L)-A1)*PI(L)-B1*PIM1(L)
      PIM1(L)=PI(L)
      PI(L)=PIP1
      WI=WI+PIP1*PIP1
  210 CONTINUE
      B1=WI/WII
      BETA(I+2)=B1
      WII=WI
      I=I+1
      GO TO 160
  302 DO 310  L=2,16
  310 G(L)=ZER
      G(1)=ONE
      DO 350 J=1,K
      S1=ZER
      DO 320 L=1,K
      G(L)=G(L)-ALPHA(L)*G(L-1)-BETA(L)*G(L-2)
```

```
      S1=S1+S(L)*G(L)
  320 CONTINUE
      C(J)=S1
      L=K
      DO  340 I2=2,K
      G(L)=G(L-1)
  340 L=L-1
  350 G(1)=ZER
      IF (NR1) 404,405,404
  404 PRINT 905, (J-1,C(J),J=1,K)
  905  FORMAT  (8E12.5)
  405 CONTINUE
      IF (CHECK) 1050,1050,1051
 1051 PRINT 1035
 1035 FORMAT (26HCOEFFICIENTS ARE ***                              )
      LPP=LP+1
      PRINT  1036,  (C(I),I=1,LPP)
 1036 FORMAT      (10E12.5)
```